



# A Regional Surface Wind Model for Mountainous Coastal Areas

James E. Overland  
Matthew H. Hitchman  
Young June Han

Pacific Marine Environmental Laboratory  
Seattle, Washington

June 1979

**U. S. DEPARTMENT OF COMMERCE**  
**Juanita M. Kreps, Secretary**

National Oceanic and Atmospheric Administration  
Richard A. Frank, Administrator

Environmental Research Laboratories  
Boulder, Colorado  
Wilmot N. Hess, Director

## NOTICE

Mention of a commercial company or product does not constitute an endorsement by NOAA Environmental Research Laboratories. Use for publicity or advertising purposes of information from this publication concerning proprietary products or the tests of such products is not authorized.

(Order by SD Stock No. 003-017-00461-9)

# CONTENTS

Abstract . . . . .	1
1. INTRODUCTION . . . . .	1
2. THE MODEL . . . . .	2
3. DETAILS OF THE MODEL . . . . .	3
3.1 Finite Difference Form . . . . .	3
3.2 Boundary Conditions . . . . .	3
3.3 Flooding . . . . .	4
3.4 Entrainment . . . . .	4
3.5 Initialization . . . . .	4
4. SIMPLE EXPERIMENTS . . . . .	4
4.1 Onshore Flow with Flat Topography . . . . .	5
4.2 Offshore Flow with Flat Topography . . . . .	6
4.3 Modification of Flow by a Coastal Mountain . . . . .	7
5. SIMULATION FOR PUGET SOUND/STRAIT OF JUAN DE FUCA . . . . .	9
5.1 Regional Description . . . . .	9
5.2 Data Sources . . . . .	9
5.3 Model Simulations . . . . .	11
5.3.1 Cyclonic Storm System . . . . .	13
5.3.2 Interior High Pressure . . . . .	13
5.3.3 Offshore High Pressure . . . . .	26
6. ACKNOWLEDGMENTS . . . . .	32
7. REFERENCES . . . . .	32
APPENDIX: Derivation of Boundary Layer Equations . . . . .	33



# A REGIONAL SURFACE WIND MODEL FOR MOUNTAINOUS COASTAL AREAS\*

James E. Overland, Matthew H. Hitchman,  
and Young June Han

*ABSTRACT.* A mesoscale numerical model of the planetary boundary layer (PBL) was modified for application to mountainous regions along the northwestern coast of the contiguous United States and the southern coast of Alaska. The model treats the PBL as a one-layer primitive equation system solving for boundary layer height, potential temperature, and the two components of horizontal velocity. Input parameters are the large-scale geostrophic wind pattern and the stability of the air mass. Experiments with a cross-section version of the model were performed to assess its response to variable terrain, differential heating, and differential roughness at the coast for a domain containing both a flat coastal plain and low coastal mountains. The complete model was applied to three quite dissimilar meteorological situations for the Puget Sound/Strait of Juan de Fuca system in northwestern Washington state. The model is specifically useful in suggesting the relative roles of inertia and topography.

## 1. INTRODUCTION

A major limitation of coastal marine meteorology is the inadequate specification of the local wind field at the spatial resolution necessary to resolve wind drift, local waves, and vessel or oil-spill leeway. Typically, this is due to the difficulty in estimating nearshore wind fields directly from large-scale synoptic patterns or from widely scattered and often unrepresentative wind measurements. Near the coastline, topography and discontinuities in surface roughness and heating give rise to significant mesoscale variations. Strong ageostrophic winds exist in the passes of the southeastern Alaskan coast and are attributed to channeling around islands. The open coast is also subject to anomalous winds caused by high coastal mountains. Of particular importance are winds blowing off the land, called katabatic winds, forced by the contrast of warm ocean temperatures and cold temperatures 50-100 km inland. Farther south, in the Puget Sound basin in Washington, forecasters are aware of a quiet zone of reduced winds in the lee of the Olympic Mountains. This zone changes location as a function of the offshore wind direction. Sea breeze circulation is an

additional example of coastal wind modification.

This report documents the combined use of a numerical meteorological model and a field measurement program to explore regional wind patterns. Within the context of its formulation, the model can be used to assess how changes in large-scale flow, surface parameters, and assumed dynamics affect the wind pattern in a limited region. A major goal is the ability to infer local winds and small-scale spatial variations in wind fields from the large-scale flow pattern for locations where long-term observations are not practical.

We have chosen to adapt the mesoscale numerical model of the planetary boundary layer (PBL) proposed by Lavoie (1972, 1974; see also Keyser and Anthes, 1977). Lavoie treats the PBL, typically 0.5 to 2.0 km deep, as a one-layer, vertically integrated primitive equation model. The model solves for boundary layer height, potential temperature, and the two components of horizontal velocity, throughout a limited region. Large-scale geostrophic wind, surface elevation, temperature, and the stability of the air in the layer above the PBL are specified as boundary conditions. Air temperature and PBL height are specified along the inflow boundaries. The local response is calculated by specifying smooth initial

\*Contribution No. 366 from the NOAA/ERL Pacific Marine Environmental Laboratory.

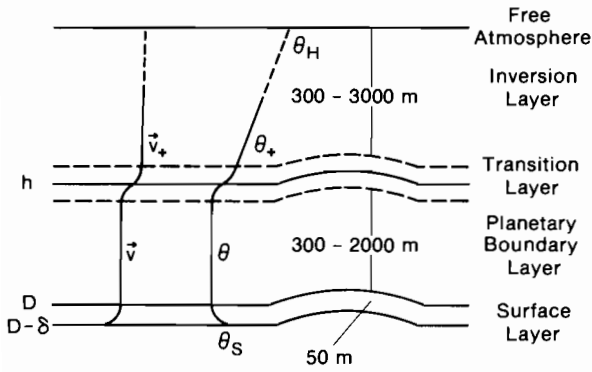


Figure 1.—Model-defined parameters of height, velocity, and potential temperature.

values of wind, temperature, and PBL height, and then time-stepping the equations of continuity, momentum, and heat conservation until a state of equilibrium is obtained. The system allows estimation of mesoscale wind variations caused by contrasts in heating and roughness of land and water, modification of the down-wind environment by advection, and channeling by topography for a given static large-scale pressure pattern. Since the model considers only one layer, processes that depend upon vertical structure cannot be directly resolved. For example, questions remain on the adequacy of the model to represent sea breeze circulation without explicitly resolving return flow aloft. However, the model is well suited to estimating wind patterns in mountainous regions with strong orographic control.

The Puget Sound/Strait of Juan de Fuca region in northwestern Washington was chosen for a test basin because there was a fairly comprehensive data set available for comparison. Since the model is quickly dominated by complex topography, several cases with simple geometry, based on a topography similar to that of western Oregon, are included in Section 4 to build confidence in interpreting more complicated results. The question of the type and quality of large-scale pressure field input is also addressed by comparison of prepared sea level pressure analysis with computer-generated objective analysis from the National Meteorological Center.

## 2. THE MODEL

The atmosphere is represented by four layers defined by changes in the lapse rate of potential temperature, as shown in fig. 1. The layer in con-

tact with the surface is a constant stress or surface layer assumed to be represented by a logarithmic velocity profile. The upper limit of this layer is taken to be 50 m. Above the surface layer is the planetary boundary layer (PBL), represented by vertically integrated values of velocity and potential temperature. The PBL is capped by a density discontinuity, which parameterizes the restoring force of an inversion layer of stable air above the PBL. The PBL is the only layer that is explicitly modeled. The model specifies four dependent variables: the PBL height,  $h$ , identified with the inversion base in unstable or neutral stratification; the PBL potential temperature,  $\theta$ ; and the two components of the vertically integrated wind velocity within the PBL,  $u$  and  $v$ , represented here by the vector  $\bar{v}$ . The governing equations for conservation of mass, momentum, and heat result from vertically integrating the primitive equations for the PBL, treating the lower atmosphere as a Boussinesq system. Interactions with the surface layer and upper atmosphere are parameterized. The resulting equations (see appendix) reduce to

$$\frac{\partial h}{\partial t} + \nabla \cdot (h-D) \bar{v} = E, \quad (1)$$

$$\begin{aligned} & \frac{\partial (h-D) \bar{v}}{\partial t} + \nabla \cdot (h-D) \bar{v} \bar{v} + (h-D) f \bar{k} \times \bar{v} \\ &= -(h-D) \bar{F}_i + \frac{g(h-D) \Delta \theta}{\theta_0} \nabla h \\ &+ \frac{g(h-D)^2}{2\theta_0} \nabla \theta + E \bar{v}_+ - C_D |\bar{v}| \bar{v}, \quad (2) \end{aligned}$$

$$\begin{aligned} & \frac{\partial (h-D) \theta}{\partial t} + \nabla \cdot (h-D) \bar{v} \theta \\ &= E \theta_+ - C_H |\bar{v}| (\theta - \theta_s). \quad (3) \end{aligned}$$

The right side of the mass conservation equation (1) represents the recruitment of mass into the PBL through entrainment of the overlying fluid at rate  $E$ . The height of the top of the surface layer above sea level is indicated by  $D$ , so that  $h-D$  is the local PBL thickness. The thickness of the surface layer is  $\delta$ . In the momentum equation (2), the second term is inertia;  $f$  is the Coriolis parameter;  $g$  is gravity;  $\theta_0$  is a reference temperature;  $\bar{v}_+$  is the velocity at the base of the inversion layer (entrained into the PBL at rate  $E$ ), and  $C_D$  is the surface drag parameter. The temperature increase between the PBL and the inversion layer is  $\Delta \theta$ . The air stability associated with the inversion is thus modeled as a jump condition in density.  $\bar{F}_i$  represents the uni-

form pressure gradient associated with the background large-scale flow (the major input to the model), while the next two terms consider pressure gradients induced by the local variations in PBL height and temperature. In the absence of mesoscale variation, (2) reduces to a geostrophic balance modified by surface drag. The right-hand side of the heat equation (3) indicates that the PBL can be warmed by entrainment at the top of the PBL ( $\theta_+$  being the temperature at the base of the inversion) or by surface heating proportional to the difference between the PBL air temperature,  $\theta$ , and the surface temperature,  $\theta_s$ .

The wind velocity  $\bar{v}$  is an average for the entire PBL. Since almost all wind shear is confined to the surface layer, the model wind can be taken as nearly equal to the wind at 50 m elevation. At this level the wind speed is approximately 15% greater than the wind measured at the normal anemometer height of 10 m. Corrected for height in this manner, the model winds should correspond to 30-min averaged anemometer winds, which are not unduly influenced by surface features smaller than the mesh length of the model for a well-mixed PBL.

### 3. DETAILS OF THE MODEL

#### 3.1 Finite Difference Form

The chosen grid is a single Richardson lattice (fig. 2) in which the  $u$  and  $v$  components are staggered relative to the height field and each other. This approach is optimal for gravity waves. This lattice also eliminates over-specification of boundary conditions, a difficulty with Lavoie's original formulation. The flux form of the advective terms maintains conservation of scalar quantities. Upstream values, rather than centrally averaged values, for advected quantities are chosen to maintain the transportive property, which guarantees one-way flow of information.

#### 3.2 Boundary Conditions

Specification of boundary conditions for limited-area integrations of the primitive equations is a formidable task. One advantage of the present approach is that constant values on the boundaries can be specified, with the integration run until all the ringing of the time-dependent modes is frictionally damped.

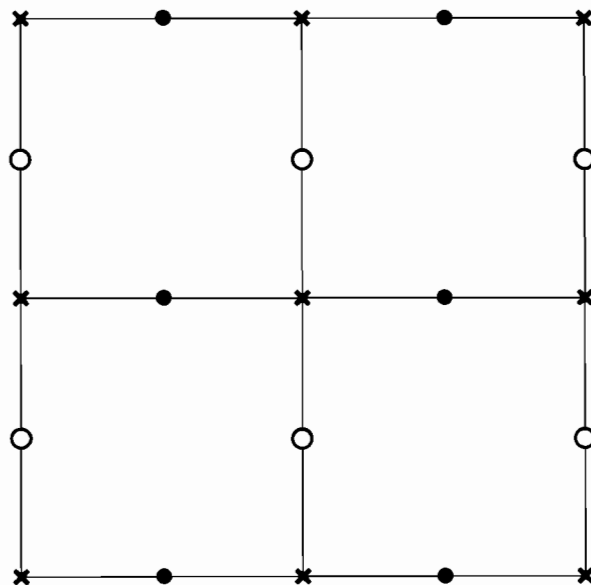


Figure 2.—Staggered mesh for primary variables. Mesh locations specify the following variables: x—temperature ( $\theta$ ) and PBL height ( $h$ ); o— $v$  component of velocity; •— $u$  component of velocity.

For domain sizes on the order of several hundred kilometers it is important to emphasize the gravitationally controlled circulation, which requires specification of either boundary layer height or inflow velocity. Along inflow boundaries over the ocean, we have chosen to specify constant PBL height,  $h_i$ , and air temperature,  $\theta_i$ . These values are held fixed for all time. Inflow boundaries over land specify the PBL height and temperature as

$$\begin{aligned} h &= h_i + aD, \quad a = 0.5, \\ \theta &= \theta_i, \end{aligned} \quad (4)$$

subject to a minimum PBL height. This minimum was set at 300 m. After the  $h$  values are set by (4), they are smoothed twice to remove the influence of rapid variations in the ground elevation  $D$ . The model needs to be rerun on a case-by-case basis, adjusting the constant  $a$  to minimize the influence of the open boundary on the height field at interior points. The authors are currently experimenting with setting the PBL height along inflow boundaries from the results of a one-dimensional model. At outflow boundaries we follow Lavoie by setting the PBL height and potential temperature at their upstream values.

Specifying the momentum flux through the open boundaries for the non-linear advection terms in the momentum equations must be done with care, because advection in a limited domain

is significant. Several options for inflow velocities were investigated, including specifying the laterally homogeneous solution for the given geostrophic wind and drag coefficient. This proved unsatisfactory because the imbalance between the boundary values and the internal values influenced by orography caused severe geostrophic adjustment problems throughout the model domain and resulted in large deviations in the height field. Our final choice is to assume zero gradient conditions on the velocity components at the inflow boundary. This assumption results in determination of the values at the first interior point by the local dynamic balance. This decision is consistent with the limited data input available and the desire to resolve orographic control interior to the model. Since upstream differencing is used for momentum advection, only minor difficulties are encountered at outflow boundaries.

### 3.3 Flooding

In the presence of high mountains or low mean velocities, the top of the marine inversion layer may actually intersect the topography. For the vertically integrated model, this is equivalent to forming an island.

In the cases studied by Lavoie it was not necessary to resolve this feature, but it must be resolved for such cases as those of Puget Sound and the high Alaskan coastal mountains. In the present model flooding is accomplished by selectively removing a grid point if the PBL depth falls below a preset value, and adding points if the surrounding PBL heights are great enough to increase the PBL depth above a minimum. Since adding or dropping points creates new internal boundary conditions, flooding increases the relaxation time to steady state by a factor of three.

### 3.4 Entrainment

Even in the absence of mountains, determination of the PBL height is a complex problem. For unstable boundary layers the height cannot be explicitly determined, but is governed by a rate equation that considers free and forced convection, large-scale subsidence, shear instabilities, and solar radiation. The importance of entrainment is problem-dependent and we can suppose that it is more significant in the Gulf of Alaska in winter, for example, with cold air outbreaks over warm water, than in Puget Sound.

In our initial application to mountainous regions we will assume that an oceanic PBL height can be specified a priori and, for the time interval necessary for a parcel to flow through the domain of the model, that no significant modification is contributed directly through entrainment, i.e.,  $E$  is set to zero. Entrainment can be added to this type of model (Stull, 1976, for example), but represents a major complication and is of secondary importance relative to the influence of large topographic features.

## 3.5 Initialization

The values of parameters and input conditions in table 1 are used in subsequent model runs.

The background large-scale pressure gradient,  $\bar{F}_i$ , is calculated to balance the specified geostrophic wind,  $v_g$ . The PBL height is initialized by  $h_i$  and velocities are initialized by 70% of the geostrophic wind.

## 4. SIMPLE EXPERIMENTS

In the sections to follow, complex topography dominates the flow field through the overlapping influence of several mountains and the contrasts between land and water. These all contribute to local modification of the wind field. To aid in interpretation of more complex results, we first describe several experiments with simple topography, isolating particular physical processes. The examples use a one-dimensional version of the model (i.e., north-south derivatives are set to zero) with the parameters given in table 1. The experiments consider either a flat topography with a land/ocean discontinuity or a mountain barrier 700 m in elevation located adjacent to the

Table 1.—Input parameters

Parameter	Value
$g$	980.6 cm sec <sup>-2</sup>
$f$	$1.08 \times 10^{-4}$ sec <sup>-1</sup>
$C_D$ (water)	$1.5 \times 10^{-3}$
$C_H$ (water)	$1.5 \times 10^{-3}$
$C_D$ (land)	$9.0 \times 10^{-3}$
$C_H$ (land)	$7.0 \times 10^{-3}$
$\Delta\theta$	3.0 K
$\theta_0$	281 K
$h_i$	600 m
$\Delta x$	3 km
$v_g$	13 m s <sup>-1</sup>
$E$	0

coastline. The model is assumed to run from west to east, with the ocean to the west. While the latter topography is fictional, it is roughly comparable to a slice through the Coast Range in Oregon. The total domain is large (300 km) to reduce the influence of the inflow or outflow boundaries. The grid mesh is 3 km. While most of the conclusions in this section can be derived from analytic solutions or scale analysis, we take the numerical approach consistent with development of the two-dimensional model.

#### 4.1 Onshore Flow with Flat Topography

Figure 3a shows the simplest case of onshore flow for a flat coastline. Geostrophic wind approaches from the left ( $270^\circ$ ) at  $13.0 \text{ m s}^{-1}$  with a boundary layer height of 600 m and no contrast between the temperatures over land and water. Seaward, the horizontally homogeneous solution matches the analytical solution for a momentum integral (Brown, 1974) with the boundary layer wind 0.96 of geostrophic and an inflow angle of  $17^\circ$ . Coastal influence begins near the shoreline and, inland, results in a PBL height increase of 260 m and a reduction in wind speed to  $9.0 \text{ m s}^{-1}$ . One measure of the relaxation distance for the flow to return to a near geostrophic-frictional balance is given by the ratio of the magnitude of the inertia terms ( $u\partial u/\partial x$ , etc.) to the large-scale pressure gradient force ( $f\bar{v}_g$ ). This ratio is given as the top curve in fig. 3a; it is largest just landward of the coast and is 0.1 at a distance of 100 km inland. Near the outflow boundary the solution again fits Brown's solution for the increased drag coefficient over land. For mass continuity in a one-dimensional model with no entrainment, the product of the  $u$  component of velocity and the PBL depth must be constant throughout the model domain. In the example of fig. 3a, conservation is satisfied to better than 0.2%.

The importance of momentum advection is further illustrated by contrasting 3a with 3b. In fig. 3b, the same conditions are specified as in 3a, except that the momentum advection terms are set to zero, leaving large-scale and locally induced pressure gradients and friction as the only forces. The seaward extent of coastal influence is much greater. The main feature, induced by the rise in the PBL height, is a coastal jet of  $14.5 \text{ m s}^{-1}$  from  $226^\circ$ , nearly a  $65^\circ$  change from the offshore direction. Another important feature is a nearly complete frictional equilibrium landward of the coast-

line. Clearly, in the absence of heating and mountains, inertia dominates onshore flow, resulting in almost no modification of the marine wind until it reaches the coastline.

The third example (fig. 4) is a sea breeze with a background geostrophic wind of  $3.0 \text{ m s}^{-1}$  from  $290^\circ$ . The land temperature is 291 K, 10 K warmer than the ocean. The temperature equilibrates to 90% of the temperature contrast 100 km inland from the coast. There is little variation in direction except for a delayed frictional turning inland. The wind speed is maximum at the coastline in response to pressure gradient induced by the land-water temperature difference. Continuity in this model requires a lowering of the PBL

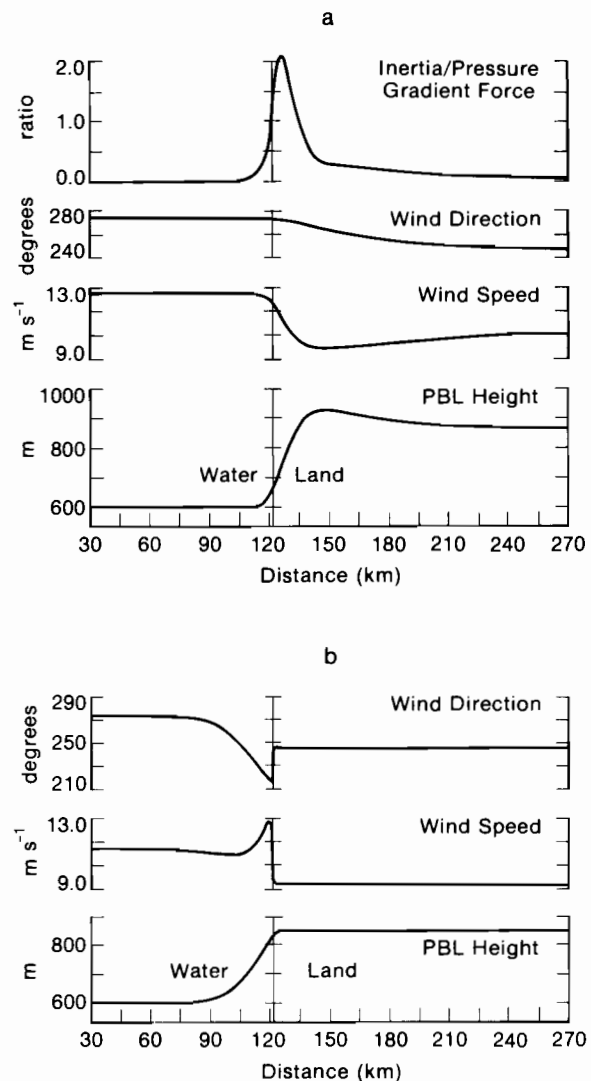


Figure 3.—(a) Onshore flow with flat coastline; (b) same case with acceleration terms set to zero.

height in the vicinity of the coast as a result of the increased velocity; the resulting slope of the PBL height influences the winds 40 km seaward of the coast. An interesting feature is the double peak in the magnitude of the inertia terms.

## 4.2 Offshore Flow with Flat Topography

Figure 5 shows an offshore wind for the same parameters as in 3a. There is acceleration across the coastline with a maximum 6 km offshore. Acceleration terms still account for 20% of the mag-

nitude of the geostrophic term at the limit of the model, 180 km seaward of the coast. Velocities over land are in frictional equilibrium but they gradually increase offshore to a super-geostrophic magnitude of  $14.6 \text{ m s}^{-1}$  at a distance of 110 km from the coast. A gradual decline is indicated near the limit of the model domain. For an overwater drag coefficient of  $1.5 \times 10^{-3}$ , the boundary layer has only begun to equilibrate with surface friction within the model domain. One can project that coastal influences of offshore flow extend seaward at least 300 to 500 km. This length scale is further substantiated by the land breeze case shown in fig. 6, in which the ocean is 10 K warmer than the land. The air temperature increases only 3 K over a distance of 180 km. The contribution of the land breeze increase over the background flow is of order  $1 \text{ m s}^{-1}$ , compared with the sea breeze-induced increase of  $3 \text{ m s}^{-1}$ . The length scale for thermal equilibrium of a coastal temperature discontinuity is well beyond the domain of the model even for modest advective velocities on the order of  $4 \text{ m s}^{-1}$ .

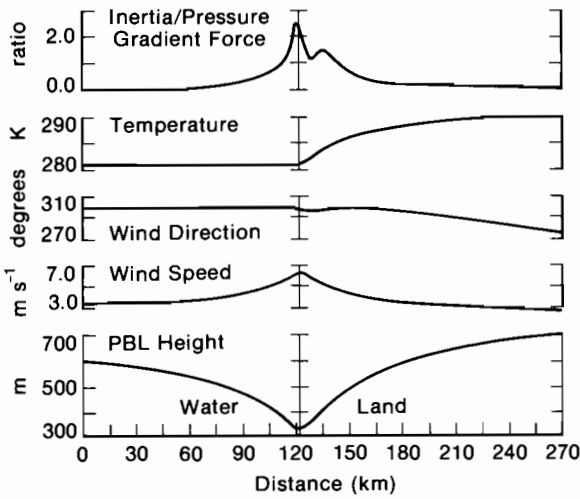


Figure 4.—Sea breeze circulation with a flat coastline.

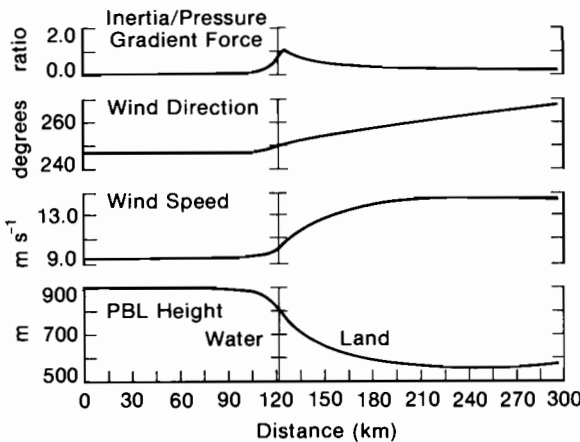


Figure 5.—Offshore wind with flat coastline.

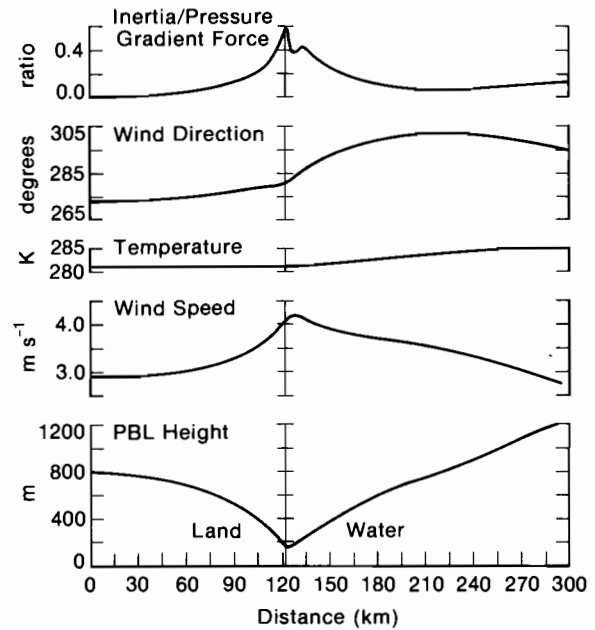


Figure 6.—Land breeze circulation with flat coastline.

### 4.3 Modification of Flow By a Coastal Mountain

Figures 7a, 7b, and 7c show the case of a coastal mountain, with onshore flow for three options of offshore PBL height and no temperature contrast. Even for moderate terrain the results are qualitatively very dissimilar to the flat coastal plain. All three cases show similar patterns of a coastal influence zone that extends from 50 to 100 km offshore. The offshore transition is not gradual, but is marked by a sharp front at the seaward limit as seen in the PBL height and magnitude of the advective terms. Within this "offshore coastal zone" the winds are reduced by as much as 40% with a minimum approximately 20 to 40 km offshore. The winds veer to the southwest as they approach the coastline and accelerate on the lee

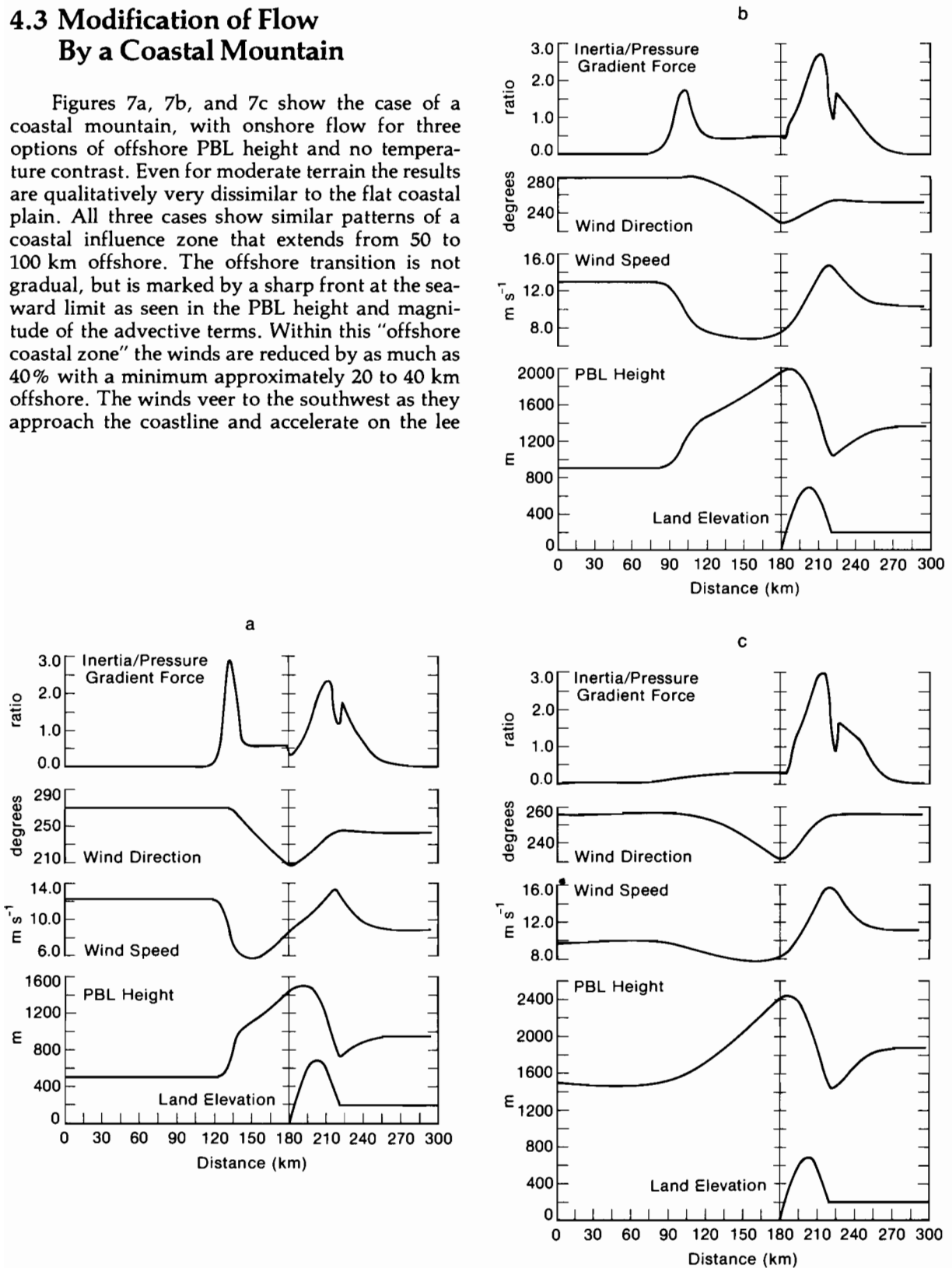


Figure 7.—Onshore flow with coastal mountain. Offshore PBL height equals (a) 500 m, (b) 900 m, and (c) 1500 m.

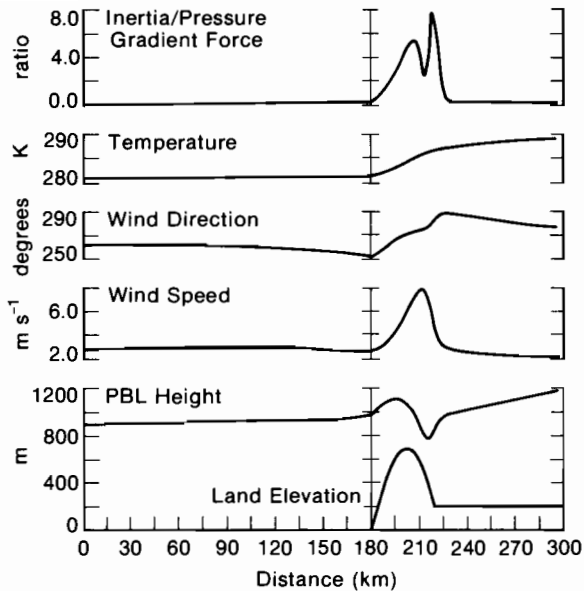


Figure 8.—Sea breeze circulation with coastal mountain.

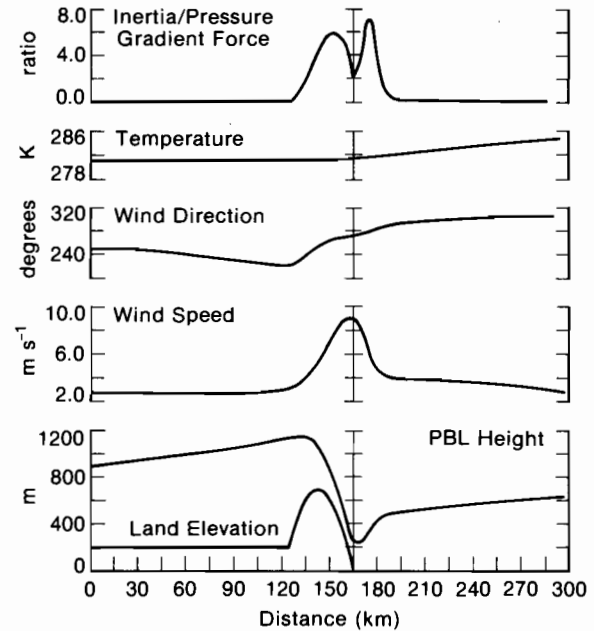


Figure 10.—Land breeze with coastal mountain.

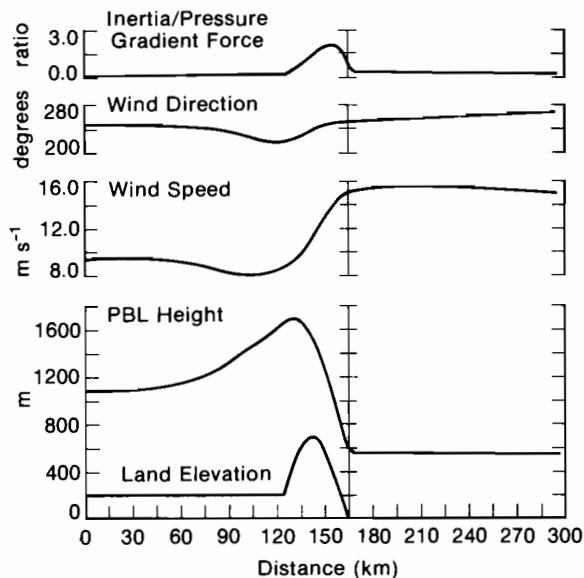


Figure 9.—Offshore flow with coastal mountain.

side of the mountain. They then recover to a near-frictional balance within 40 km of the lee side PBL minimum. Figure 8 shows the influence of the presence of the mountain on sea breeze circulation (10 K temperature contrast between land and sea). In this formulation the mountain acts as an effective barrier to development and emphasizes the importance of low-level valleys in the mountain range for the development of sea breeze circulation. In addition to temperature contrasts, flows

through valleys would be enhanced by the high pressure developed on the windward side of the ridge. Figures 9 and 10 show offshore flow and land breeze for a low coastal mountain. Unlike the onshore flow case with constant friction on the lee side of the mountain, a pronounced minimum in the PBL height does not occur when there is a reduction in friction on the leeward side of the mountain. This case strongly contrasts with the offshore flow case for flat topography in that there is virtually no variation in velocity seaward of the coastline. In the land breeze case, the temperature contrast reinforces the down-slope flow, resulting in a maximum wind speed of  $9 \text{ m s}^{-1}$  at the coast, reducing to  $4 \text{ m s}^{-1}$  at 20 km offshore.

Several important qualitative results can be inferred from the one-dimensional model runs. First, the length scale for frictional and thermodynamic equilibrium over water is several hundreds of kilometers; this is consistent with wintertime observations of outbreaks of cold continental air over the Atlantic Ocean along the northeastern coast of the United States. Second, in the vicinity of discontinuities, advective effects dominate. Third, the presence of even modest orography modifies the offshore flow pattern. One can anticipate that alongshore variations in topography are also important. Finally, except for certain special cases, observations made right at the coast should be, at best, only qualitatively similar to the offshore flow field.

## 5. SIMULATION FOR PUGET SOUND/STRAIT OF JUAN DE FUCA

A matter of primary importance is determining the transport mechanism of any petroleum spilled into the waters of Puget Sound or southeastern Alaska. Since winds have a sizable effect on surface drift, direct measurements of winds over the water are being made as part of coastal assessment programs. A goal of the regional meteorological model is to extend the usefulness of these observational data sets and to enhance the understanding of the mesoscale atmospheric response.

We have selected for modeling three generalized examples of meteorological flow conditions for the Puget Sound system. Midwinter is characterized by a series of cyclonic storms (Section 5.3.1) with strong winds from the southwest carrying warm moist air inland over western Washington. Another frequent winter case is the lull between storms, with high pressure to the east of the region (Section 5.3.2) causing strong easterly winds along the axis of the Strait of Juan de Fuca with relatively light winds elsewhere. In the summer months, anticyclonic flow around a well-developed semi-permanent high pressure cell to the west of the region (Section 5.3.3) causes prevailing northwest winds offshore along the western coasts of Washington and Vancouver Island.

### 5.1 Regional Description

The area investigated includes western Washington, the southern end of Vancouver Island, and southwestern British Columbia. Major features are the offshore ocean, Puget Sound, and the Straits of Juan de Fuca and Georgia (fig. 11). This region spans the coordinates 121°W to 126°W and 46°N to 56°N. Topographic data for the model were obtained from a master tape at the National Center for Atmospheric Research (NCAR). The mesh is a grid of 5 minutes latitude and longitude, with an average elevation computed for each square. The NCAR elevation data were smoothed in both directions (Shuman, 1957). Figure 12 presents a view of the smoothed topographic grid as seen from the southwest.

The Cascade Mountains form a north-south barrier to the east ranging from a low elevation of 916 m at Snoqualmie Pass to a high of 4392 m at

Mt. Rainier, with an average height of 1800 m. The Olympic Mountains in the center of the region rise gradually from the south and west to 2428 m at the summit of Mt. Olympus, with an average height of 1600 m, descending rapidly to the north and east. A significant area of higher elevation to the south is the Willapa Hills, 300 to 600 m high, between the Columbia River and the Chehalis River Valley. Vancouver Island is primarily mountainous, with heights averaging 900 m, reaching 1200 m in several locations.

This topography establishes one main low-level north-south passageway, extending from the Columbia River Valley through Puget Sound, and two low-level east-west passageways, the Strait of Juan de Fuca and the Grays Harbor Inlet/Chehalis River Valley area.

### 5.2 Data Sources

We obtained a set of data that adequately represent the regional wind field during the period November 1976 through January 1977. This set includes data from routine meteorological station reports and from an array of recording anemometers at strategic locations. Figure 13 and table 2 provide station locations, sources, and National Weather Service (NWS) station symbols. Teletype data for NWS offices and Coast Guard stations were obtained from the Ocean Services Unit of the Seattle Weather Service Forecast Office. The Weather Service offices and ships from the Northeast Pacific typically report every 6 h. The Coast Guard stations usually report every 3 h, but most do not report during the night. Three MRI Model 7092 Anemometers set out by the authors yielded strip charts, which were converted to 1-h averages and plotted every 6 h. Data from three vector-averaging anemometers in the Strait of Juan de Fuca were provided by the MESA Puget Sound project (Holbrook and Halpern, 1978). It should be noted that stations 10-17 in table 1 are well inland; thus, local microtopography affects the air movement there more than at the shore stations, and makes them less indicative of the general flow. Station wind reports were mapped every 6 h from 0000 Greenwich Mean Time (GMT) on 27 November 1976 to 1800 GMT on 26 January 1977. From these regional maps, examples of typical weather events were selected.

For each case selected, large-scale synoptic pressure maps centered on western Washington were prepared from North Pacific synoptic charts. In addition, objective sea level pressure analyses

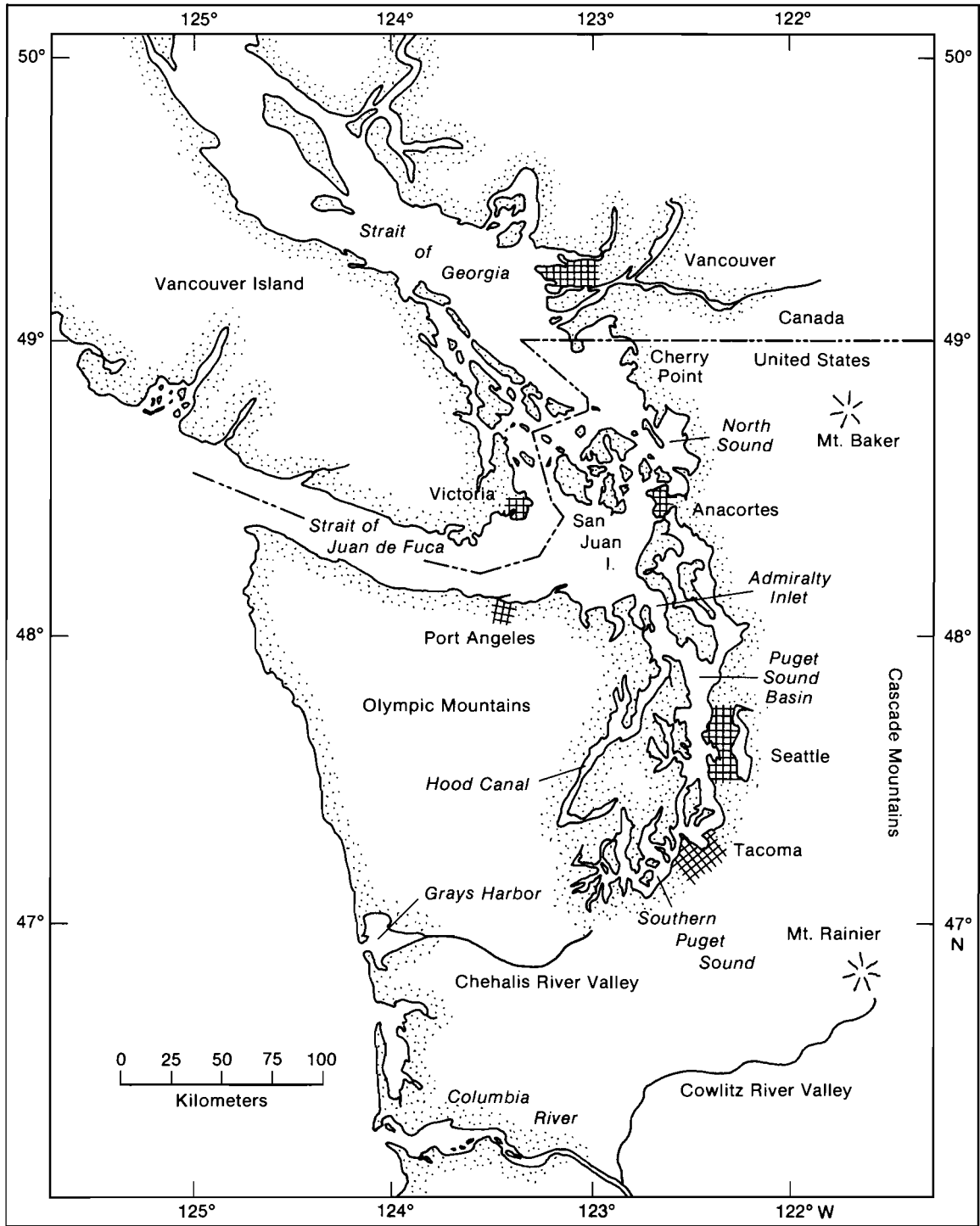


Figure 11.—The Puget Sound/Strait of Juan de Fuca region.

Table 2.—Stations used on local wind maps

Number	Station Location	Source	Symbol
1	Transient Ships	W	
2	Columbia River Weather Ship	W	NNCR
3	Astoria	W	AST-791
4	Willapa Bay	C	89S
5	Cape Shoalwater	A	
6	Westport	C	84S
7	La Push	C	87S
8	Quillayute	W	UIL-797
9	Cape Flattery	C	93S
10	North Point	W	105
11	Snider	W	109
12	South Olympic	W	138
13	Dayton	W	253
14	Wolf Point	W	572
15	Round Mountain	W	743
16	Lester	W	450
17	Little Mountain	W	432
18	Buoy 3	H	
19	Buoy 4	H	
20	Buoy 2	H	
21	Port Angeles	C	NOW
22	New Dungeness	C	96S
23	Point Wilson	C	53S
24	Point Wilson	A	
25	Smith Island		
26	Friday Harbor	C	S19
27	Victoria	W	VI-200
28	Patricia Bay	W	YJ-799
29	Cassidy Airport	W	CD-890
30	Comax	W	QQ-893
31	Vancouver	W	VR-892
32	Abbotsford	W	XX-108
33	Point No Point	C	97S
34	West Point	C	43S
35	West Point	A	
36	Alki Point	C	91S
37	Sea-Tac Airport	W	SEA-793
38	Point Robinson	C	99S

**KEY**

- C Coast Guard station report
- A PMEL land-based anemometers
- H PMEL buoy-placed anemometers
- W National Weather Service station report

on the Limited Area Fine Mesh Model (LFM) grid were obtained for the region from the National Meteorological Center. We will compare the objective analyses on the 160-km mesh to the hand-drawn charts to determine whether LFM input is adequate for the regional model. Upper-air sounding data were available from Quillayute station on the Washington coast; weather ship *Papa*, located at 50°N, 145°W; Sea-Tac airport, south of Seattle; and Portage Bay in Seattle. The pressure analysis maps show pressure in millibars, written out to the units place on isobars and to the tenths place at stations. In the latter the first two digits are deleted; e.g., 236 = 1023.6 mbar. Wind is given on these maps as barbs (one full barb = 10 kn). On the local wind maps, direction and speed to-

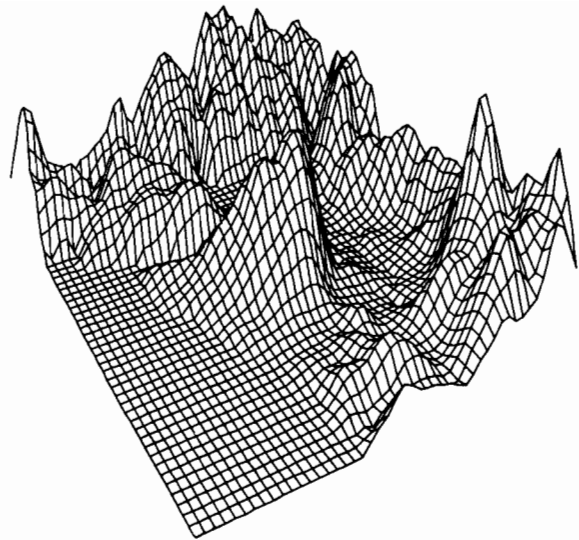


Figure 12.—Topographic grid used in the computations as viewed from the southwest.

gether are given at stations; e.g., 2813 = wind from 280°, speed 13 kn.

### 5.3 Model Simulations

Two basic regimes describe the general weather characteristics of Decembers in western Washington. As is typical of the latitude, a succession of frontal passages from the west, varying in number and intensity, dominates, producing strong winds from the southwest. Between storms, high pressure builds up near the area, often in the continental interior, bringing clear skies and relatively low winds lasting for several days to a week or more. The fall and winter of 1976 were unusual in that a persistently recurring ridge of high pressure (500 mbar) over the Northeast Pacific, frequently extending almost to the pole, allowed only an occasional weakened frontal passage through the area. Surface high pressure associated with the 500-mbar pattern, but displaced eastward over the continent, dominated the Puget Sound Basin.

We selected examples from the data set described above to model both of the basic winter regimes, the typical midwinter case (cyclonic storm system) and the frequent lull between winter storms (interior high pressure). In addition, we chose to use data from the same winter set to model the typical summer case (offshore high pressure), since, in all respects except temperature, the example selected is representative of the summer pattern.

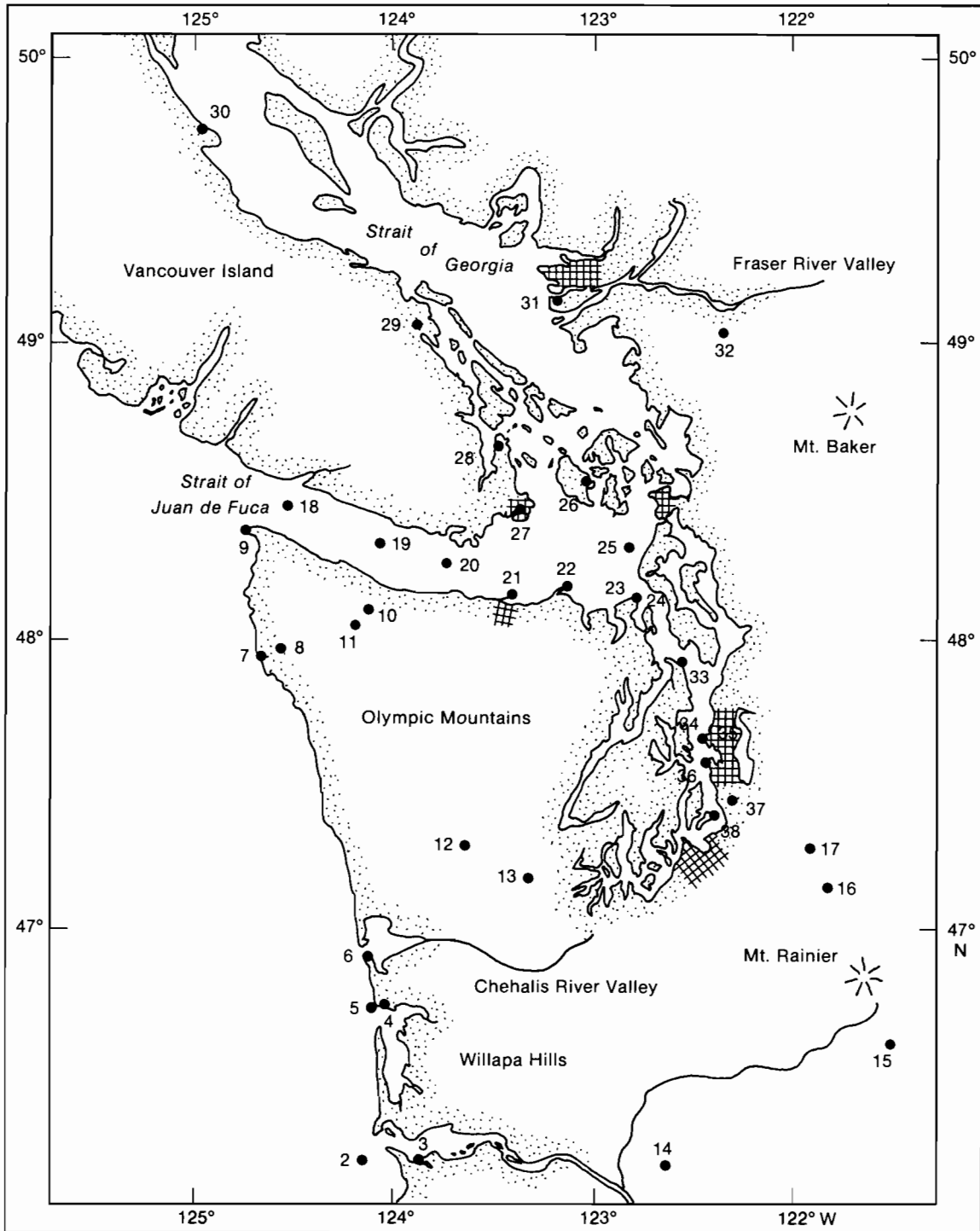


Figure 13.—Locations of anemometer stations that collected data for December 1976–January 1977.

### 5.3.1 Cyclonic storm system

The front that approached the coast at 0000 GMT, 8 December 1976 (fig. 14), turned into a cold front of respectable energy as the high retreated far to the south. The even isobars and southwesterly geostrophic flow before this front are typical before the passage of a cold front. From the local wind vectors (fig. 15), one first notices that the flow is channeled by the Olympic and Cascade Mountains. Winds over Puget Sound are stronger and more southerly than offshore. A region of light winds is evident in the lee of the Olympic Mountains. There is also general steering of the flow along the axis of the Strait of Georgia, more than a  $90^\circ$  deflection from the geostrophic wind. The temperature sounding at 1605 GMT on 7 December at Sea-Tac shows a relatively moist, deep, well-mixed PBL with near-neutral stability (fig. 16). This is illustrated further by the fact that the 850-mbar flow is very similar to the surface flow on the LFM maps (see figs. 17a and 17b). The hand-drawn and LFM surface maps agree well. Figures 18 and 19 for 0000 GMT, 15 December, show an additional example of strong winds from the southwest.

The corresponding storm situation of 8 December 1976 is simulated by a model run for PBL heights of 1800 m and 900 m (figs. 20a and 20b). Geostrophic wind is  $14.7 \text{ m s}^{-1}$  from  $251^\circ$ . The overall wind pattern for a PBL height of 1800 m is much smoother than that suggested by observations. The pattern for the lower height, however, is about as detailed as the observed pattern. An eddy has formed at the east end of the Strait of Juan de Fuca near Port Angeles in each simulation. The PBL height deviations show a gentle rise over the windward side of the mountains with a pronounced lee wave trough on the downwind side of the Olympics and Vancouver Island. With a low inversion height, increased winds flow through the low point in the mountains of Vancouver Island and spill out over the inland waters. Observed winds in the east end of the Strait of Juan de Fuca are less intense and more westerly than either model run suggests. It may be that the position of the eddy and the magnitude of the pressure gradient that develops along the axis of the Strait of Juan de Fuca are very sensitive to the volume of air channeled through Puget Sound, which depends in turn on the orientation of the offshore flow. Inflow along the southern boundary is not handled satisfactorily by arbitrary specification of inversion height, especially at the land-water interface. However, this does not appear to unduly influence the flow in the central basin.

In the previous section it was noted that

inertia plays a dominant role in mesoscale circulations. The main difference between the two model runs lies in whether the flow goes over the mountain or around it. Since observations resemble more the case with a lower inversion, perhaps the effective cross-sectional height of the mountains is higher than the model-assumed average elevations; the light stable stratification of the PBL shown in the Sea-Tac sounding may contribute to increased channeling.

### 5.3.2 Interior high pressure

A good example of interior high pressure occurred at 0000 GMT on 1 December 1976. For several days before and after this time, high pressure prevailed over southeastern British Columbia, extending north and south over the interior plateau (fig. 21). In areas of flat topography, widely spaced isobars would suggest a weak flow outward from the high pressure center westward over the area. However, the local wind shown in fig. 22 reveals a complex pattern with easterly winds at the coast and calm or light northerly winds in Puget Sound. A very interesting feature is seen in the Strait of Juan de Fuca. In sharp contrast to the weak and variable winds elsewhere on the inland waters, there is a strong flow out the Strait, reaching 20 kn at Cape Flattery. This isolated jet was reported by Reed (1931) but is not specifically mentioned in more recent literature. Associated with these low-level wind vectors are temperature soundings over the area that reveal a strongly stratified regime throughout the planetary boundary layer. The Sea-Tac sounding at 1610 GMT on 30 November 1976 is shown in fig. 23. Lines of constant potential temperature are also shown, indicating stable stratification throughout the boundary layer.

In the objective analyses from the National Meteorological Center, the absence of horizontal air flow seen at 850 mbar in fig. 24a for 1 December, 0000 GMT, contrasts with the surface pattern (fig. 24b), which shows a light pressure gradient east-west through the region in agreement with the hand-drawn map. The spacing on the surface LFM map is 1 mbar, approximately equivalent to the 10-geopotential meter spacing of the 850-mbar LFM map. The decoupling of the 850-mbar and surface layer is consistent with the strong vertical stratification observed at Sea-Tac. Stability restricts the flow to regions below the mountain tops where the air is accelerated along the east-west pressure gradient out through the Strait of Juan de Fuca and west through the Cowlitz Valley south of the Olympic Mountains. The winds are stronger in the strait than along the southern Washington

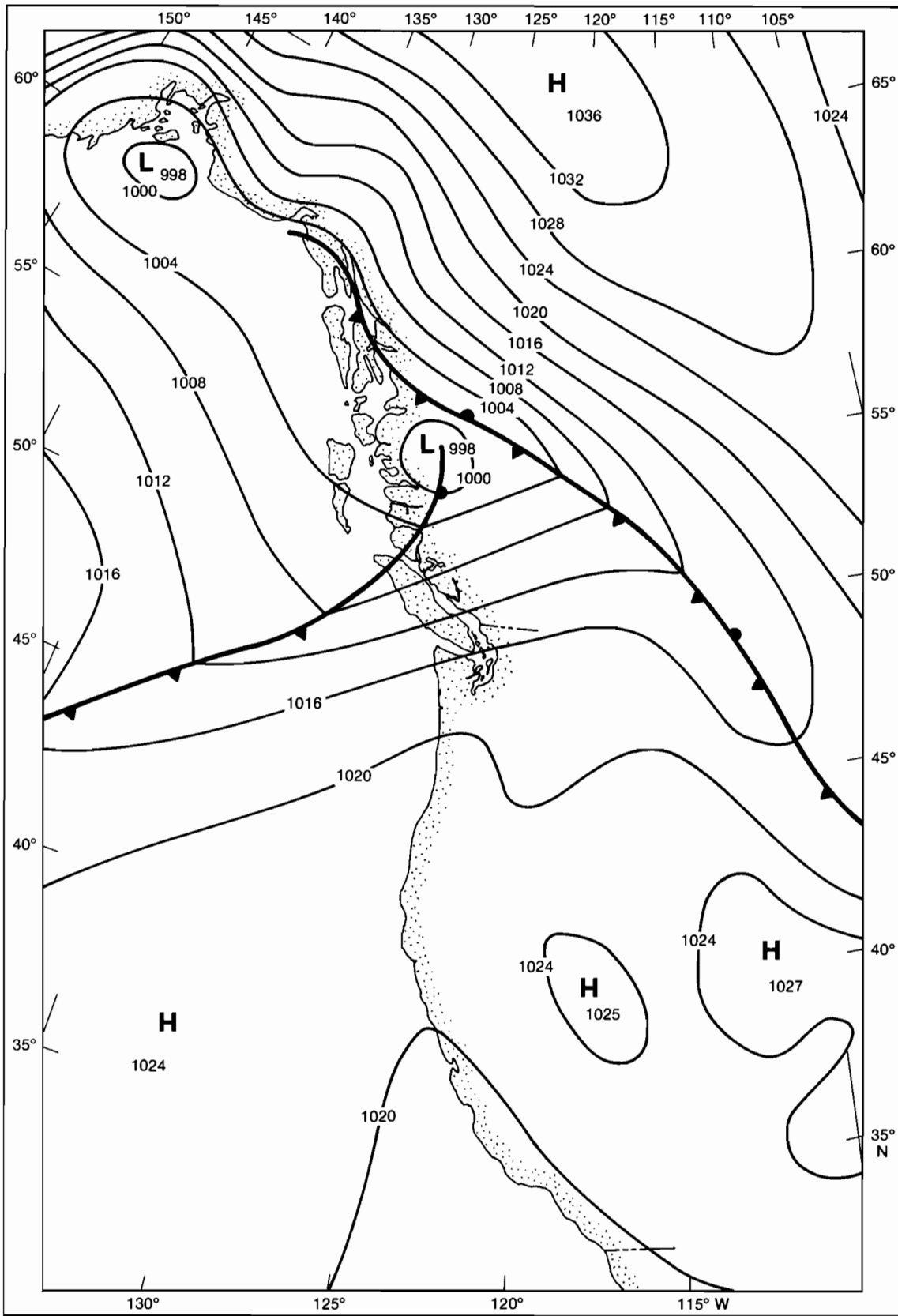


Figure 14. — Sea level pressure chart, 8 December 1976, 0000 GMT.

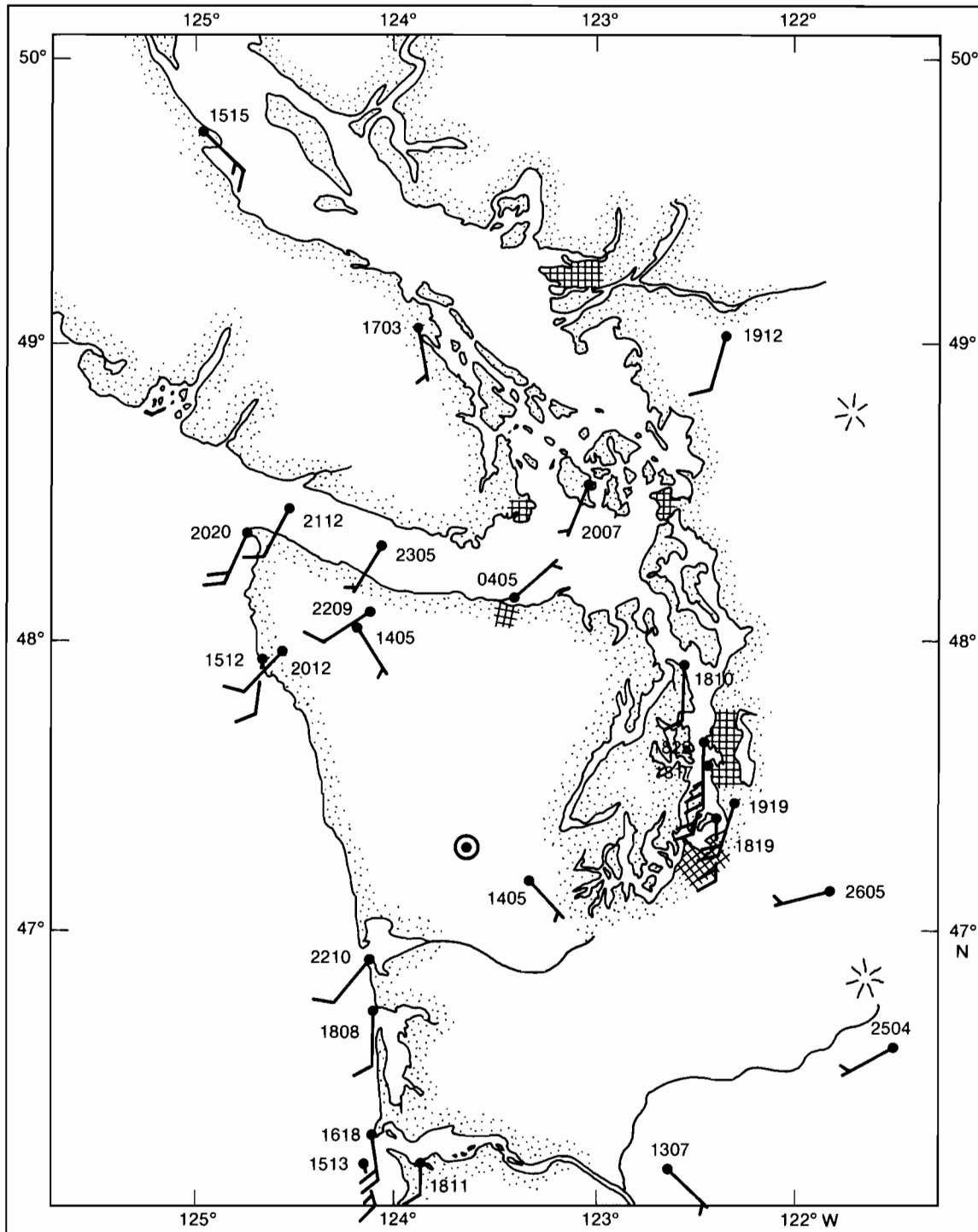


Figure 15.—Local wind observations, 8 December 1976, 0000 GMT.

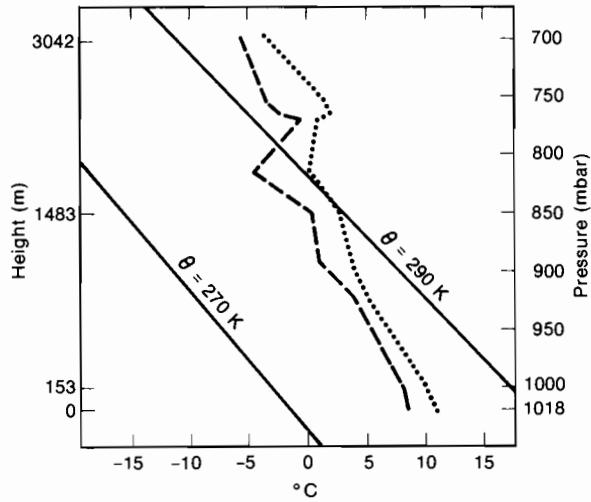
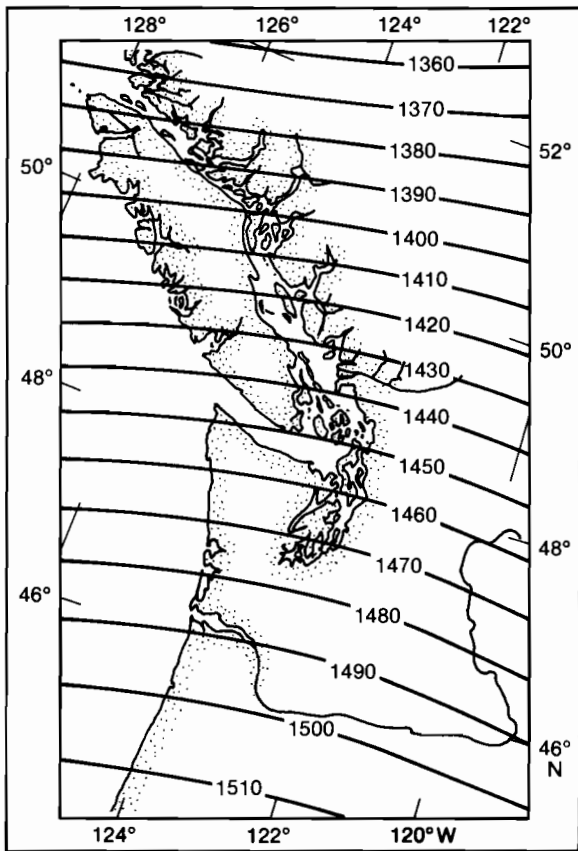
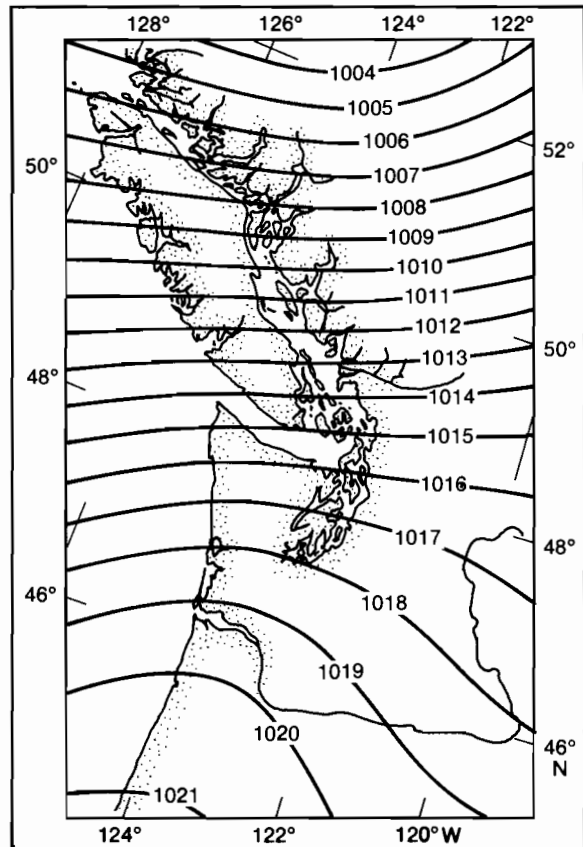


Figure 16.—Temperature sounding (· · · ·), dew point (— — —), and potential temperature (—) at Sea-Tac for 1605 GMT, 7 December 1976.



a



b

Figure 17.—Objective analysis of (a) 850-mbar heights and (b) sea level pressure on 8 December 1976, 0000 GMT.

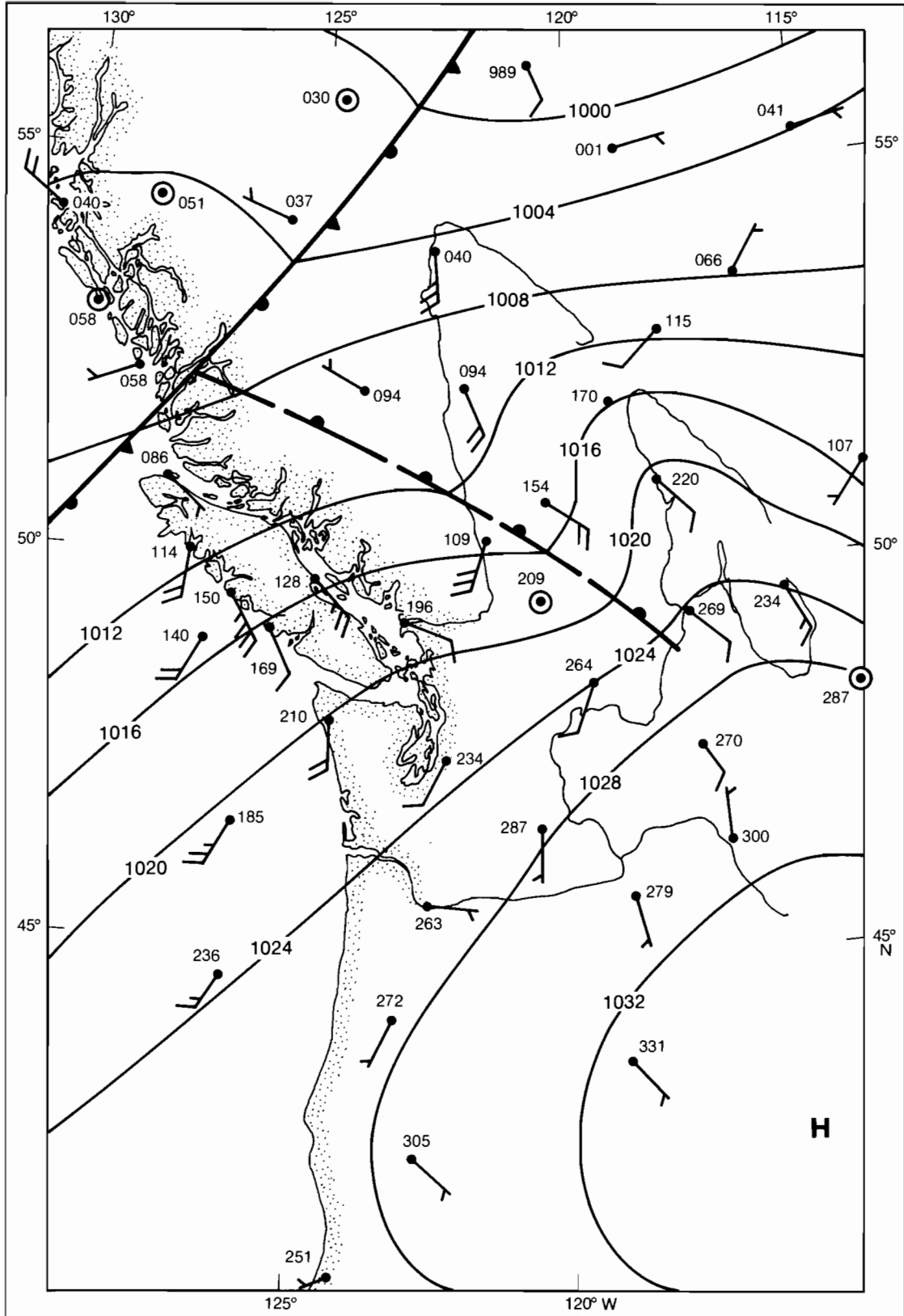


Figure 18. —Second example of strong onshore flow from southwest, 15 December 1976, 1800 GMT.

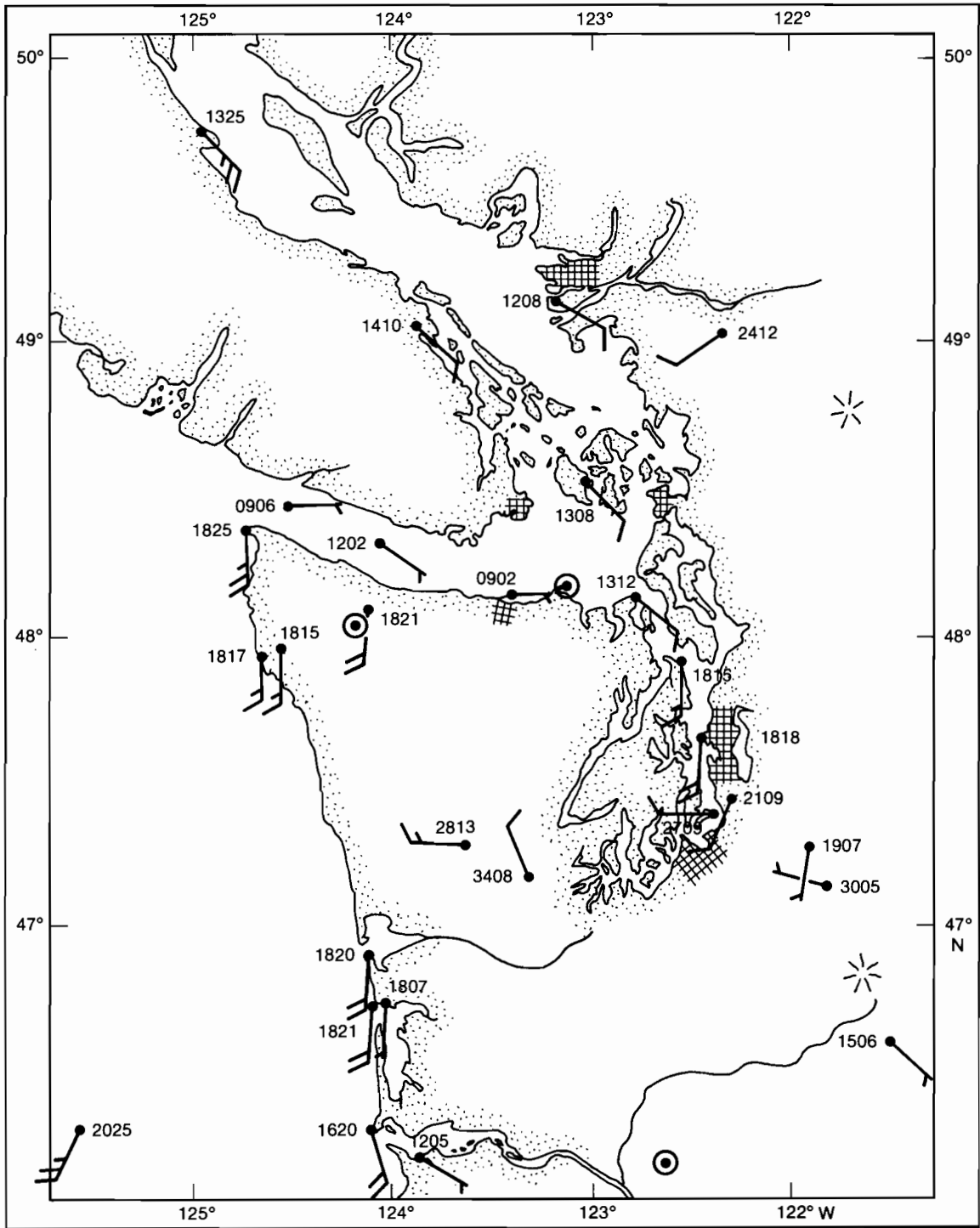


Figure 19.—Local wind observations for fig. 18.

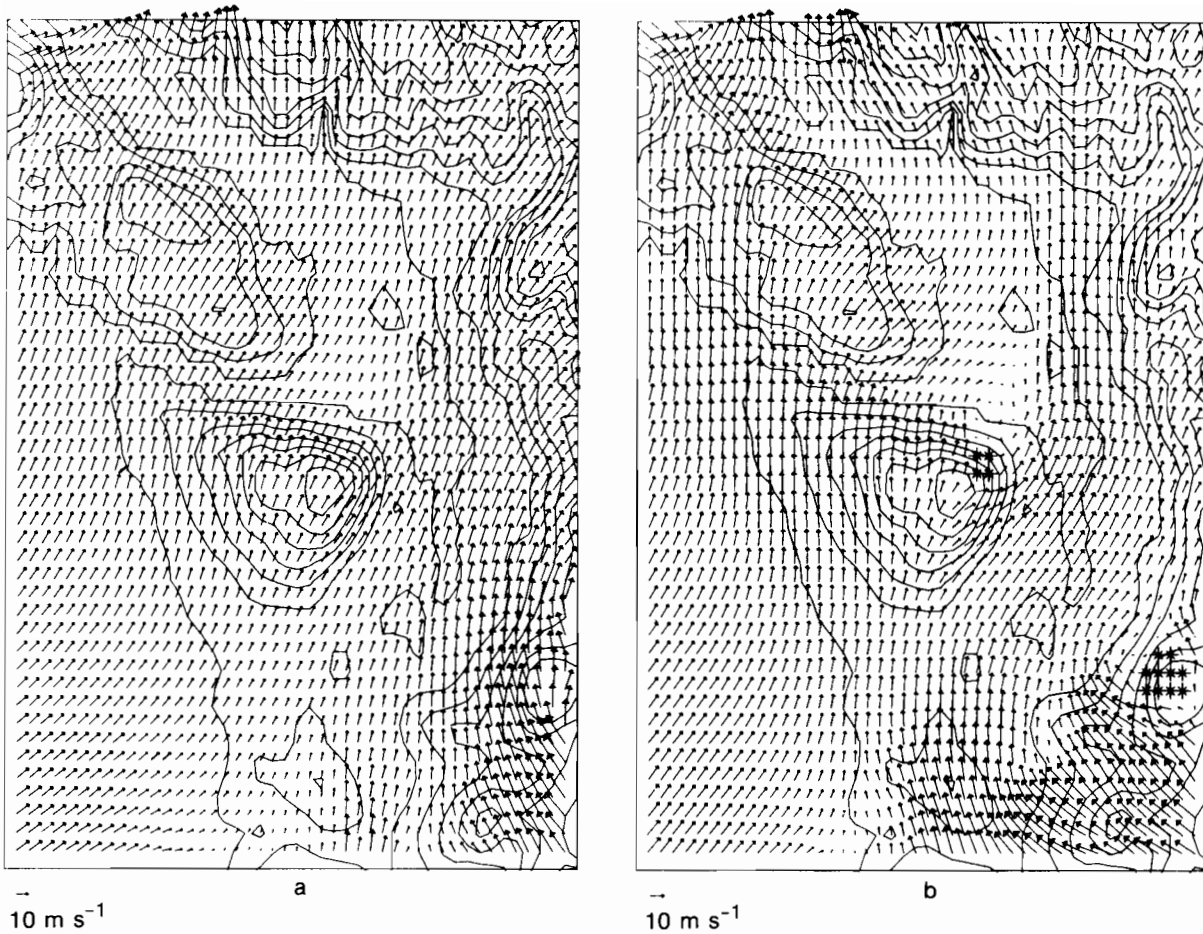


Figure 20.—Velocity vector plots of model winds for southwest flow. Offshore PBL height equals (a) 1800 m and (b) 900 m.

coast because the down-gradient acceleration is uninhibited by surface friction. Another curious feature is that the winds in Puget Sound proper flow south, in the opposite direction to those inferred from the surface geostrophic wind. A second example of winds under the high pressure regime is seen in figs. 25 and 26, where high pressure has built up rather rapidly between frontal passages. The local stations again reflect the widely spaced isobars with easterly winds on the coast, calm in the sound, and acceleration along the Strait of Juan de Fuca.

Figure 27a shows the wind pattern generated by the model corresponding to the case of 1 December 1976. Although the boundary layer is not well mixed as assumed in Section 2, we believe that we can simulate the forced channeling for the east wind case by assuming a very shallow PBL in the model, capped by very strong stability. Input parameters are summarized in table 3. The model

was initialized by a geostrophic wind of  $4.8 \text{ m s}^{-1}$  from  $144^\circ$  and a low PBL height of 0.6 km as representative of stable conditions throughout the lower troposphere. The major features are light winds in the central basin, weak easterly flow along the coast, and accelerating easterly flow down-gradient through the Strait of Juan de Fuca,

Table 3.—Model input parameters<sup>1</sup>

Wind Type	Date (1977)	Geostrophic Speed (m/s)	Wind Direction	$h_i$ (km)	$\Delta\theta$ (K)	$T_a$ (K)
E	1 Dec 00Z	4.8	$144^\circ$	0.6	9.8	273.0
SW <sub>1</sub>	8 Dec 00Z	14.7	$260^\circ$	1.8	7.0	289.5
SW <sub>2</sub>	8 Dec 00Z	14.7	$260^\circ$	0.9	7.0	289.5
NW	9 Dec 12Z	16.2	$321^\circ$	1.0	5.2	280.1

<sup>1</sup>The influence of temperature in the form of land-water temperature differences was neglected in all Puget Sound cases. Thus, it was not necessary to carry the heat equation in the calculations.

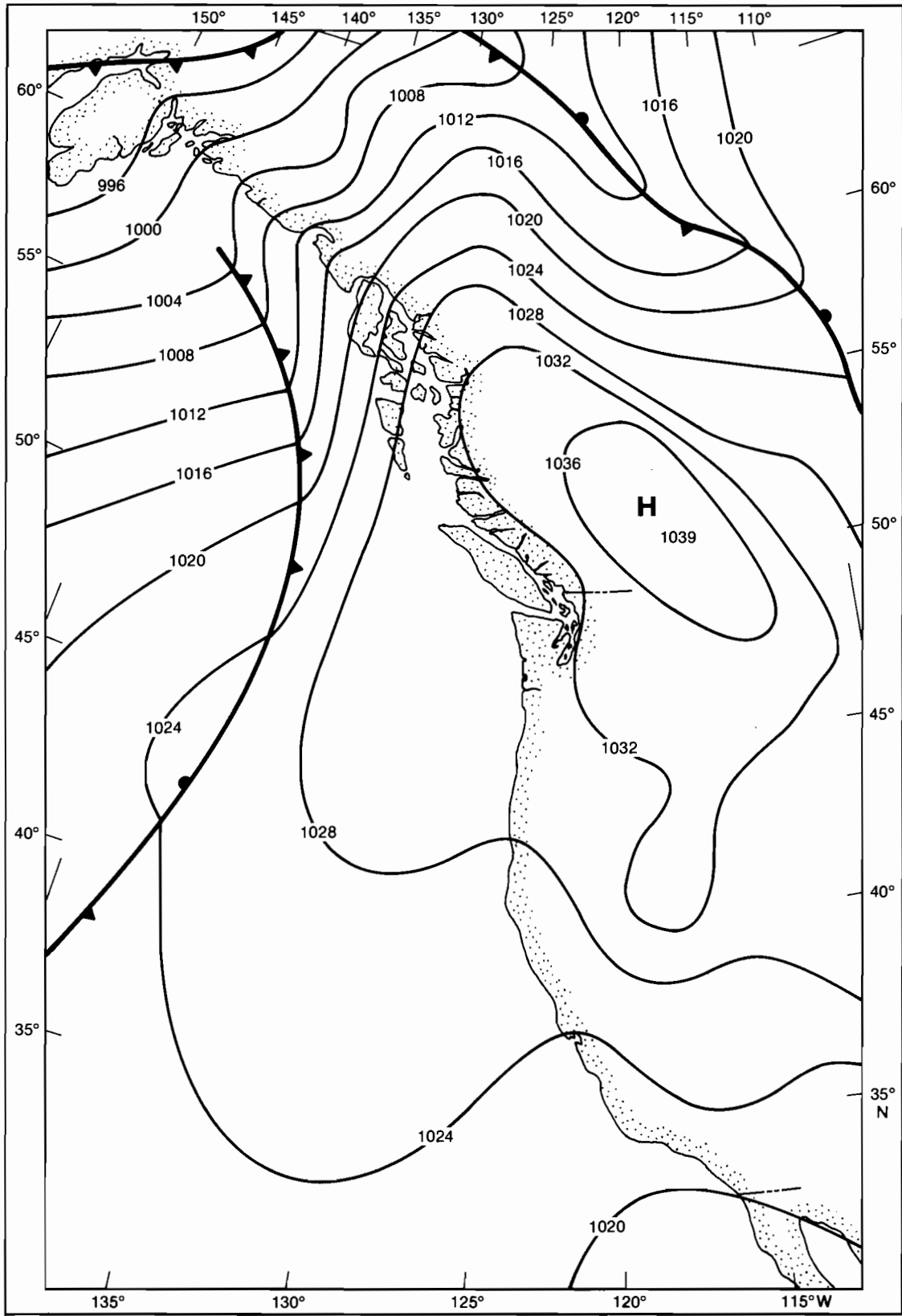


Figure 21. — Sea level pressure analysis, 1 December 1976, 0000 GMT.

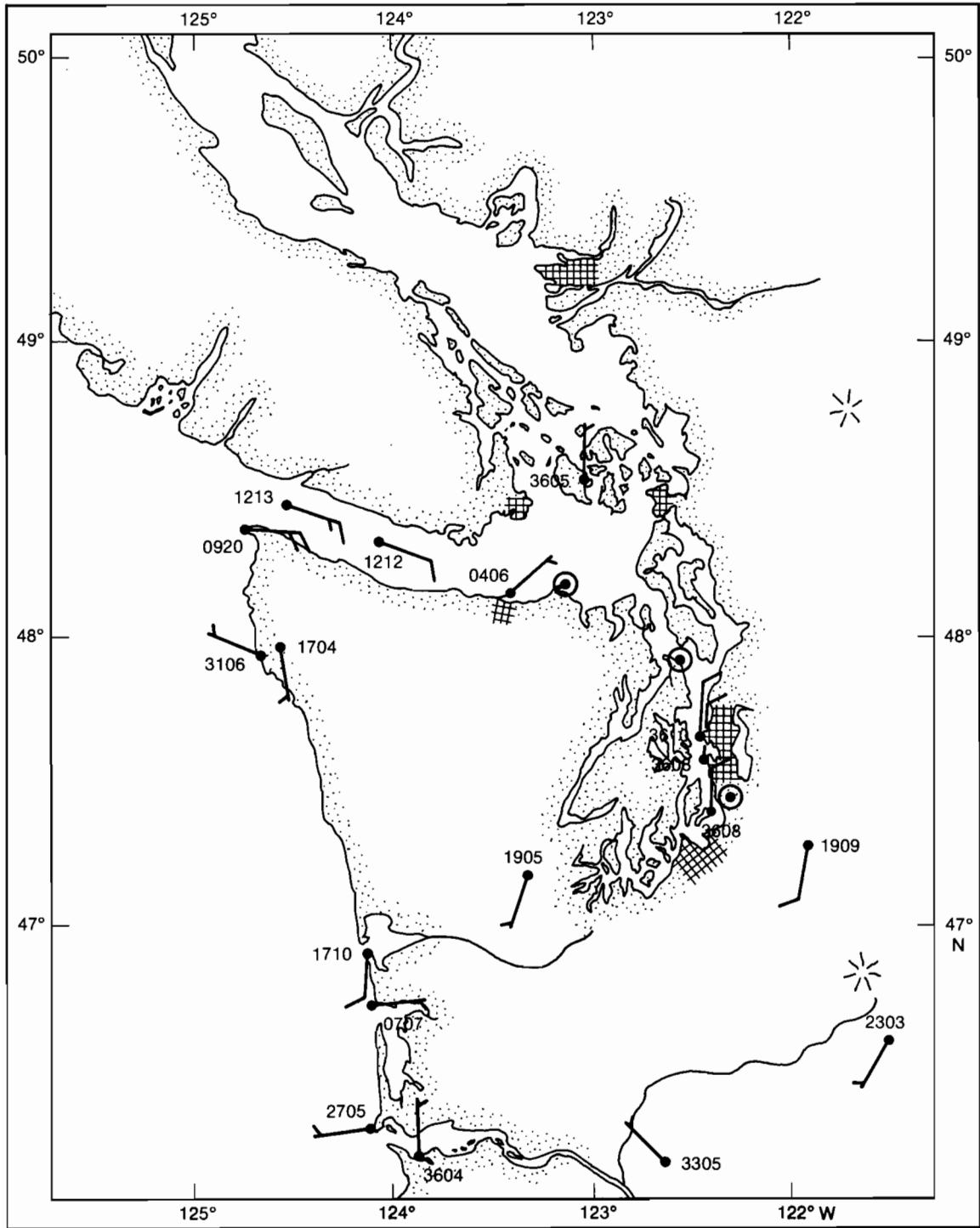


Figure 22. —Local wind observations, 1 December 1976, 0000 GMT.

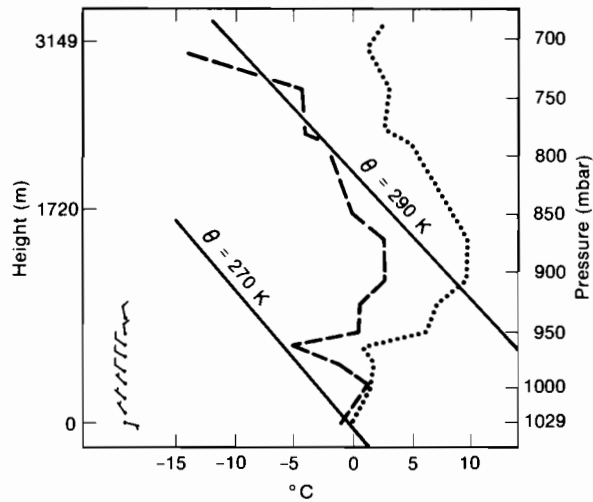
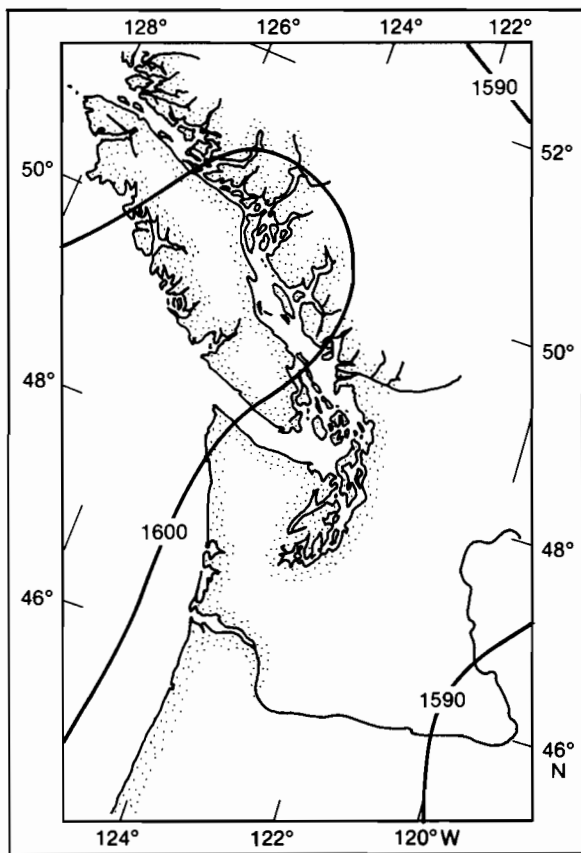
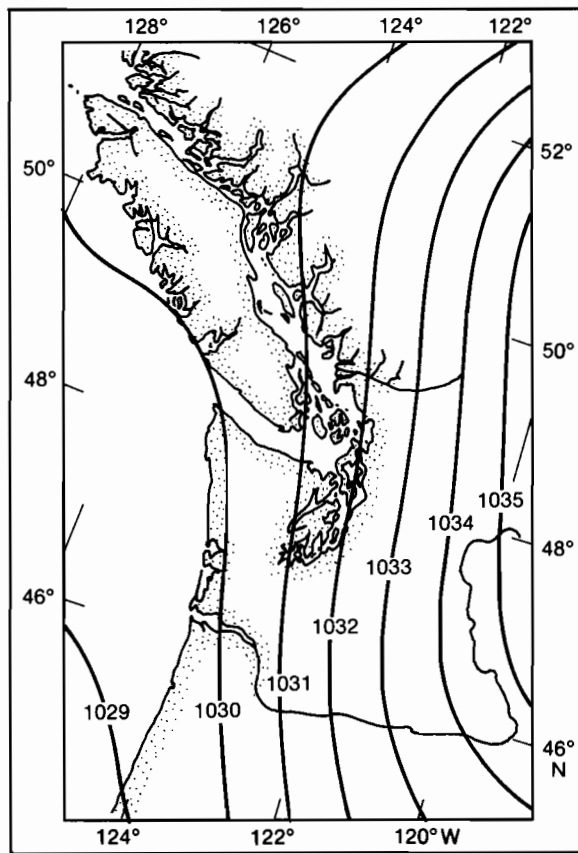


Figure 23.—Temperature sounding (· · · ·), dew point (— — —), and potential temperature (——) at Sea-Tac for 1610 GMT and wind at Portage Bay for 2015 GMT, 30 November 1976.



a



b

Figure 24.—Objective analysis of (a) 850-mbar heights and (b) sea level pressure on 1 December 1976, 0000 GMT.

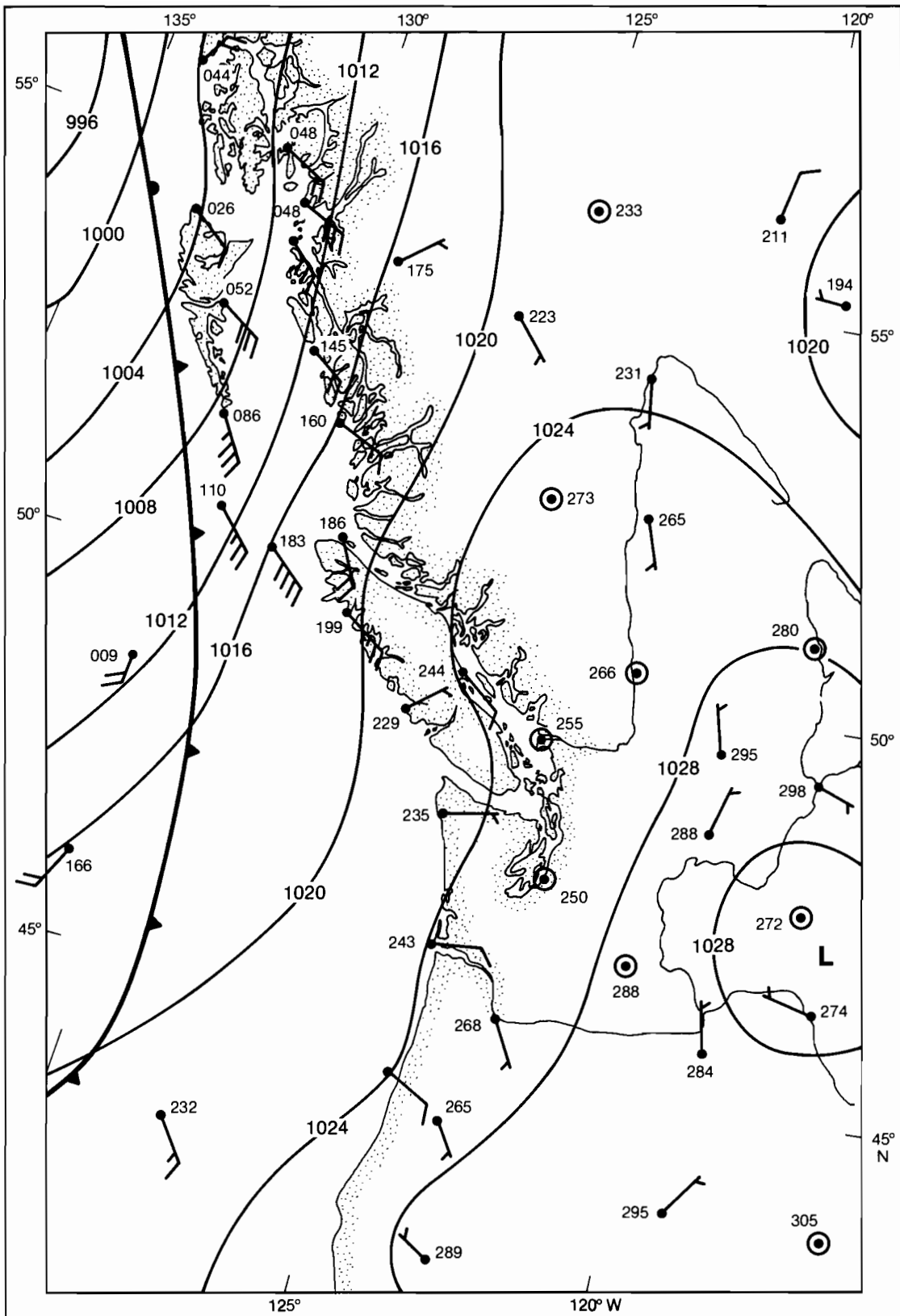


Figure 25.—High pressure to the northeast of Puget Sound, 21 December 1976, 1800 GMT.

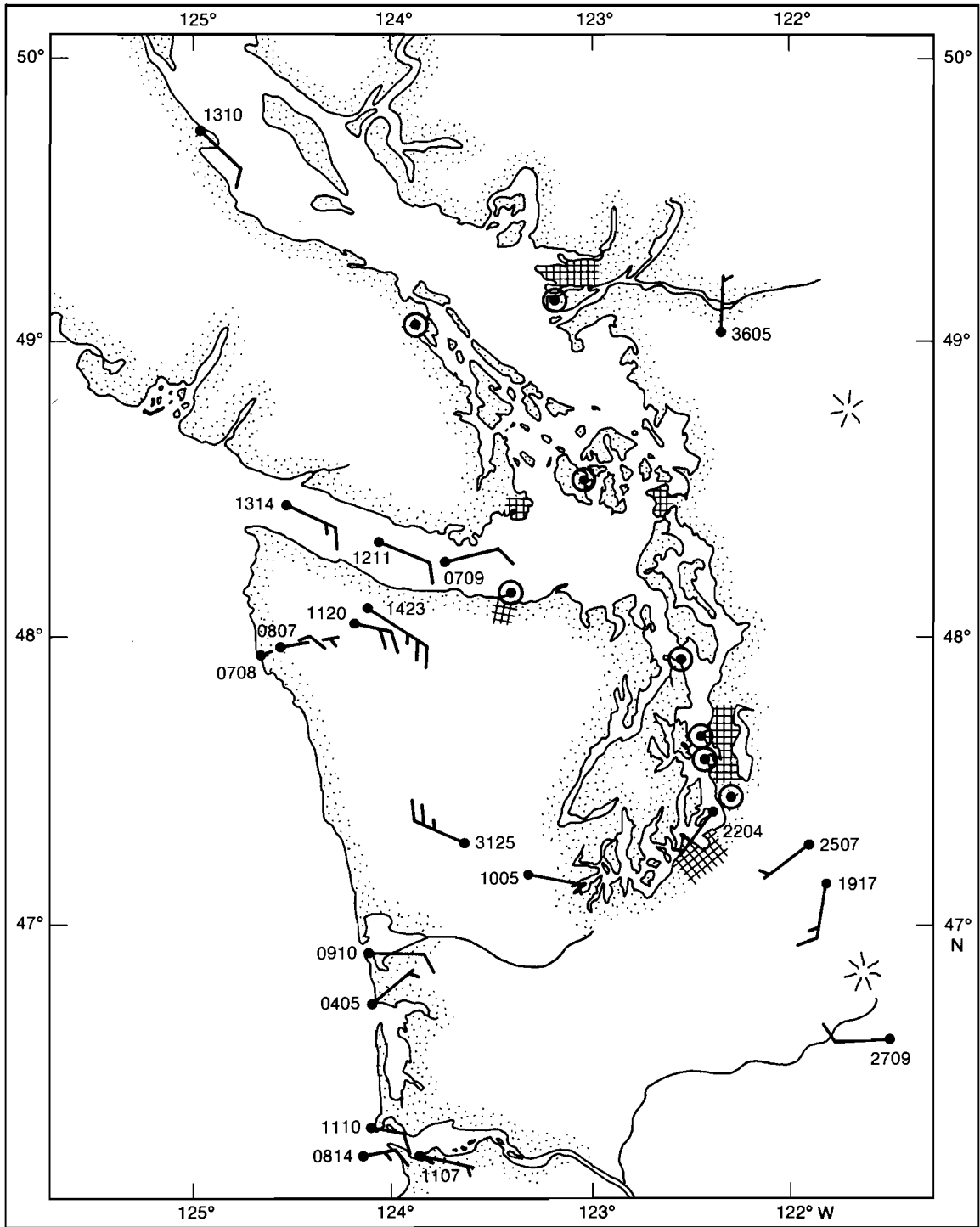


Figure 26.—Local wind observations for pressure field shown in fig. 25.

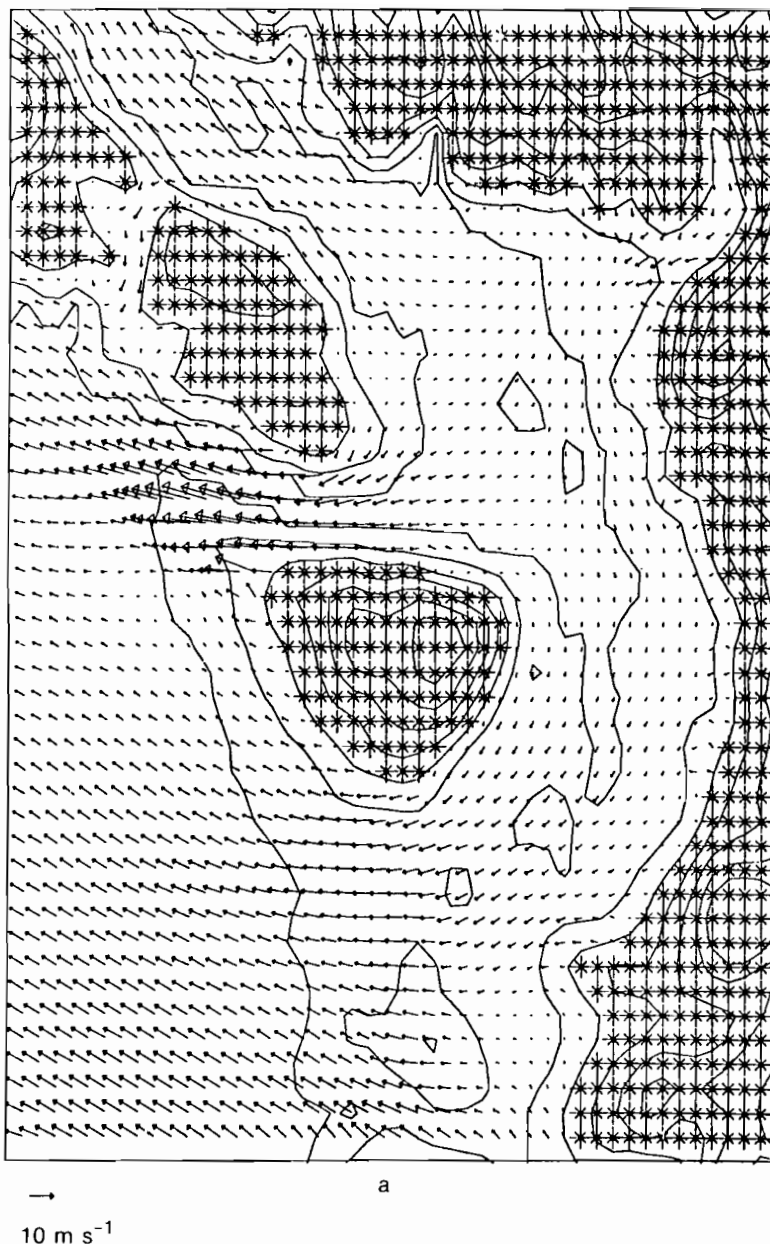
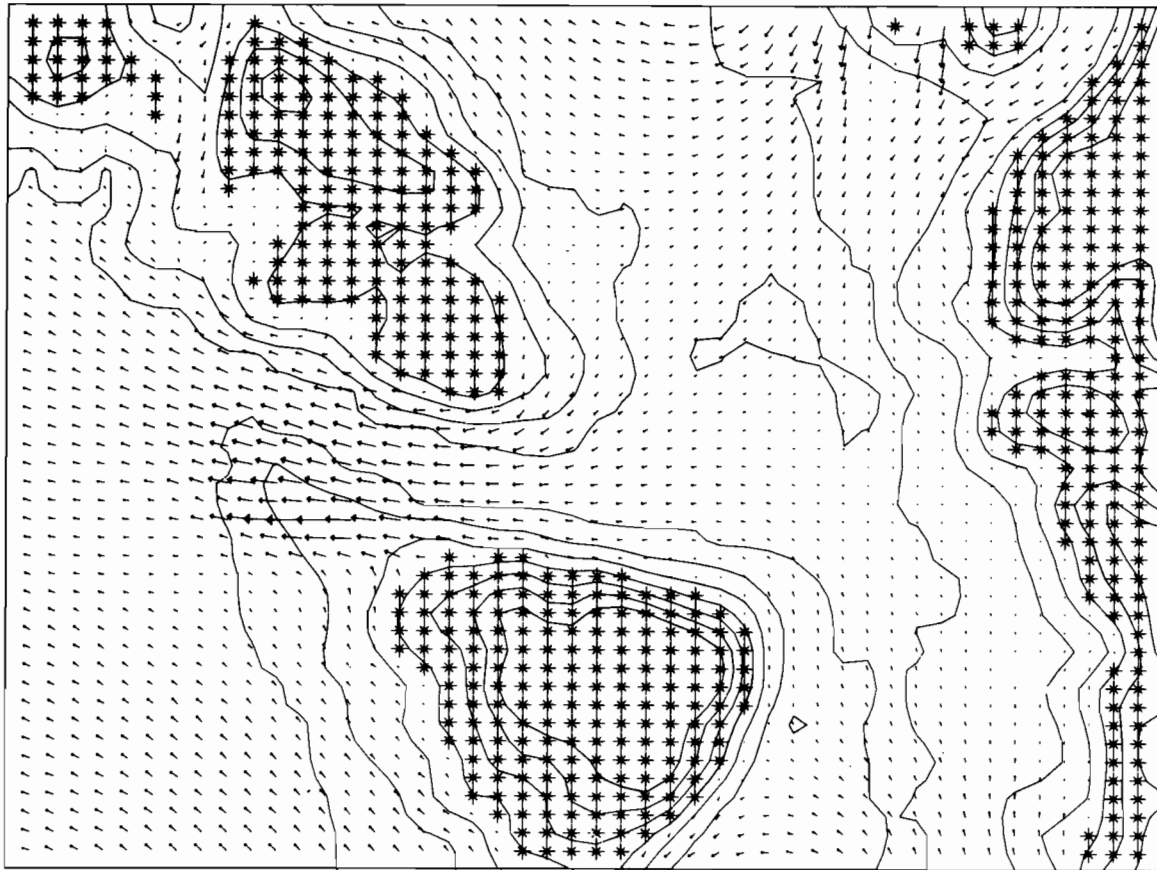


Figure 27a.—Velocity vector plot of model run for east wind case.

similar to the conditions shown in figs. 22 and 26. As the flow in all channels is out of the Puget Sound basin, this case could not be run to steady state. In the prototype the outflowing air is replaced by subsidence associated with the synoptic high pressure. Subsidence is not included in the model to balance the falling PBL height; fig. 27a is the model-estimated wind field when the interior PBL height has reached 400 m after 4 h and is falling at a constant velocity. To increase the resolu-

tion in the main area of interest, the Strait of Juan de Fuca, the grid length was reduced to one-half of its previous value in the north-south direction, and the domain was also reduced to see whether the model could be sectionalized (fig. 27b). Good agreement is obtained in the strait. Contrary to the inference from observations, at the east end of the Strait of Juan de Fuca a more geostrophic flow occurs if the southern end of Puget Sound is not included in the model domain.



10 ms<sup>-1</sup>

Figure 27b.—Velocity vector plot of model run for east wind case with increased north-south resolution.

### 5.3.3 Offshore high pressure

The front depicted in fig. 25 was the weakest of four crossing the region in December 1976. For a day following the 8 December front and a day following the 22 December front, a cell of high pressure existed off the coast of Oregon and Northern California and brought strong northwesterly winds through Washington as part of an anticyclonic circulation. Except for temperature effects, this pattern is typical of summertime conditions in the region. The hand-drawn pressure map of 1800 GMT, 23 December 1976, shows a relatively uniform pressure gradient from offshore inland to Vancouver, B.C. (fig. 28). The local anemometer readings (fig. 29) reveal the effect of topography on a northwesterly geostrophic wind. Strong channeling is indicated in the Strait of Juan de Fuca with variable winds in the lee of the Olympic Mountains. It is interesting that for this

case and for 1200 GMT, 9 December 1976 (figs. 30 and 31), there is a southerly flow in lower Puget Sound in the lee of the Olympics, but only at the surface. Figure 32 shows the wind sounding for 1400 GMT, 9 December, at McChord Air Force Base, and the Quillayute temperature sounding. The LFM maps (figs. 33a and 33b) concur with the hand analysis in showing a northwesterly geostrophic flow.

Figure 34 shows the model velocity field for northwest winds. Channeling is indicated in the Strait of Juan de Fuca and especially in the Strait of Georgia. Height deviations are less intense than for the southwest wind case, although the velocity field indicates that the lee wave eddy is still a major feature. A southerly tendency is indicated in the lower Puget Sound trough where the flow is parallel to the pressure gradient below the ridge crests.

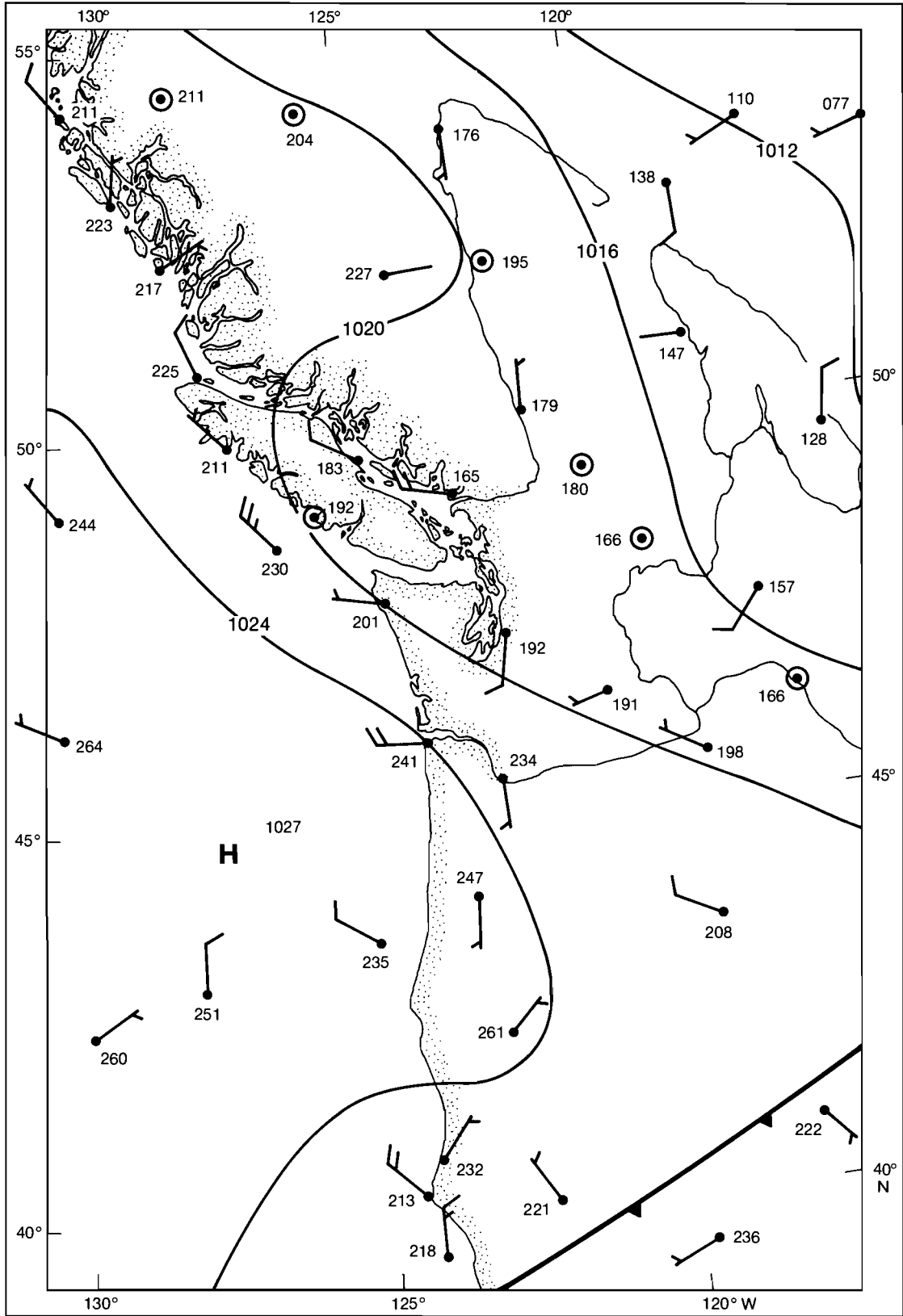


Figure 28.—Sea level pressure chart, 23 December 1976, 0800 GMT.

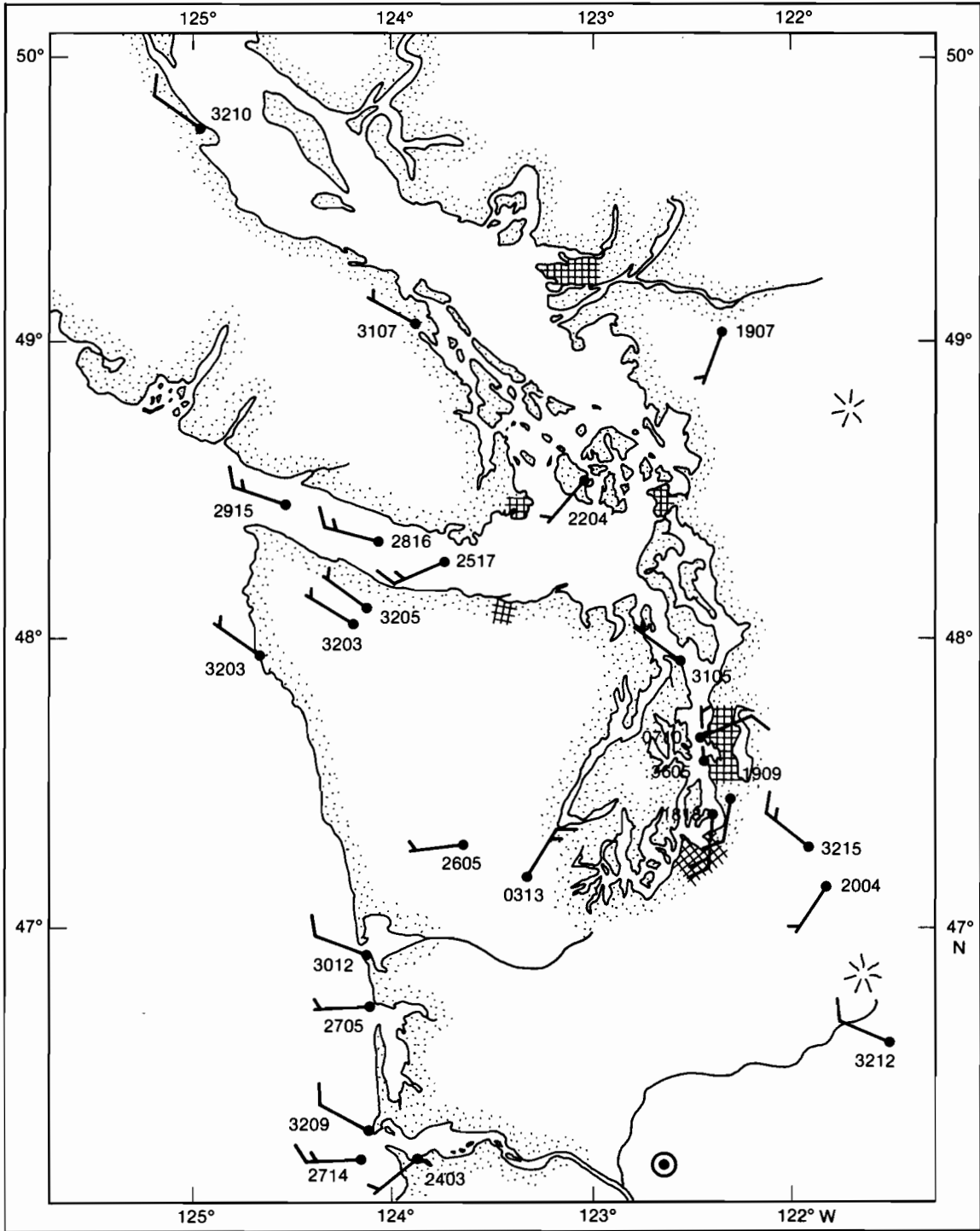


Figure 29. —Local wind observations, 23 December 1976, 1800 GMT.

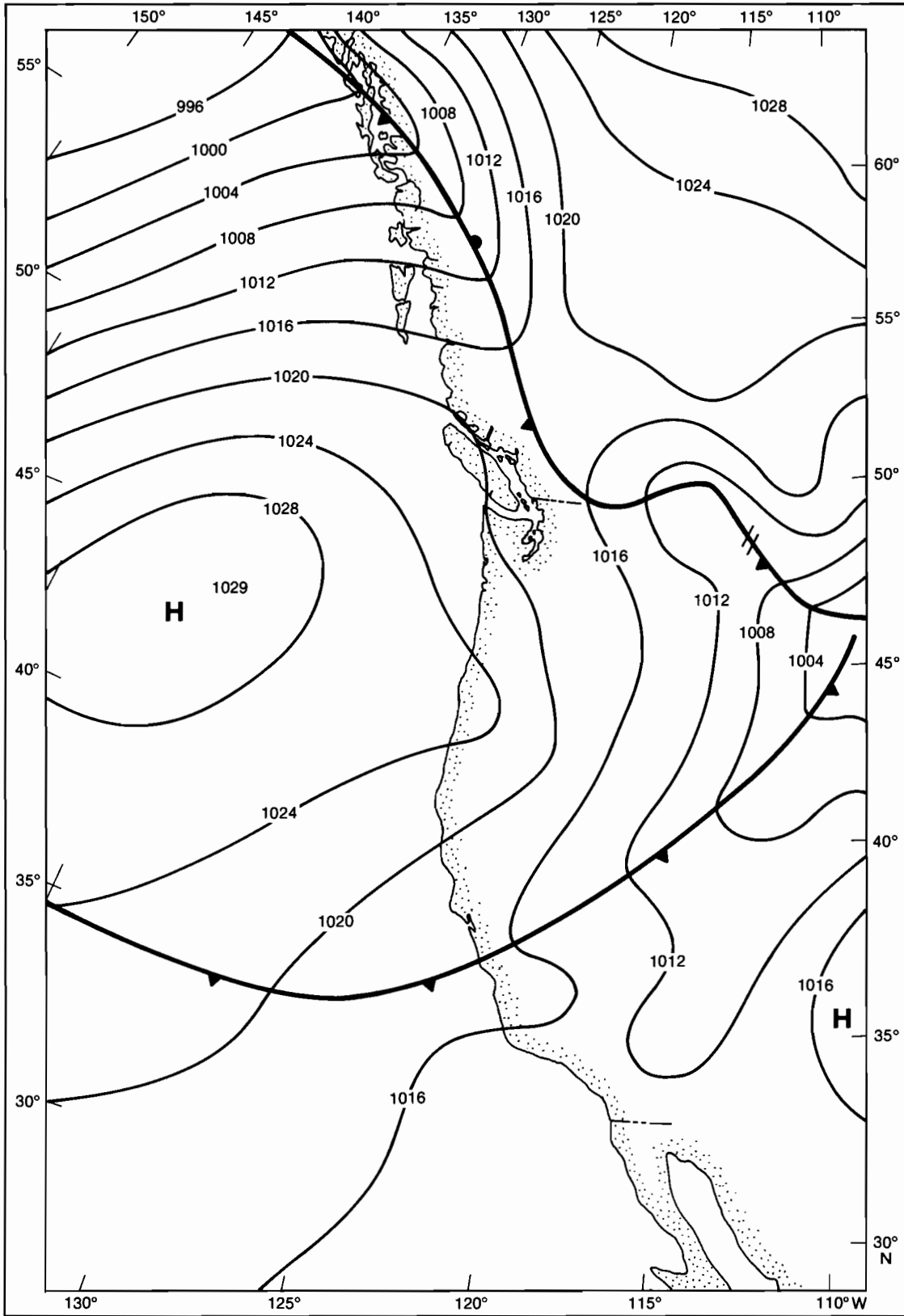


Figure 30.—Sea level pressure chart, 9 December 1976, 1200 GMT.

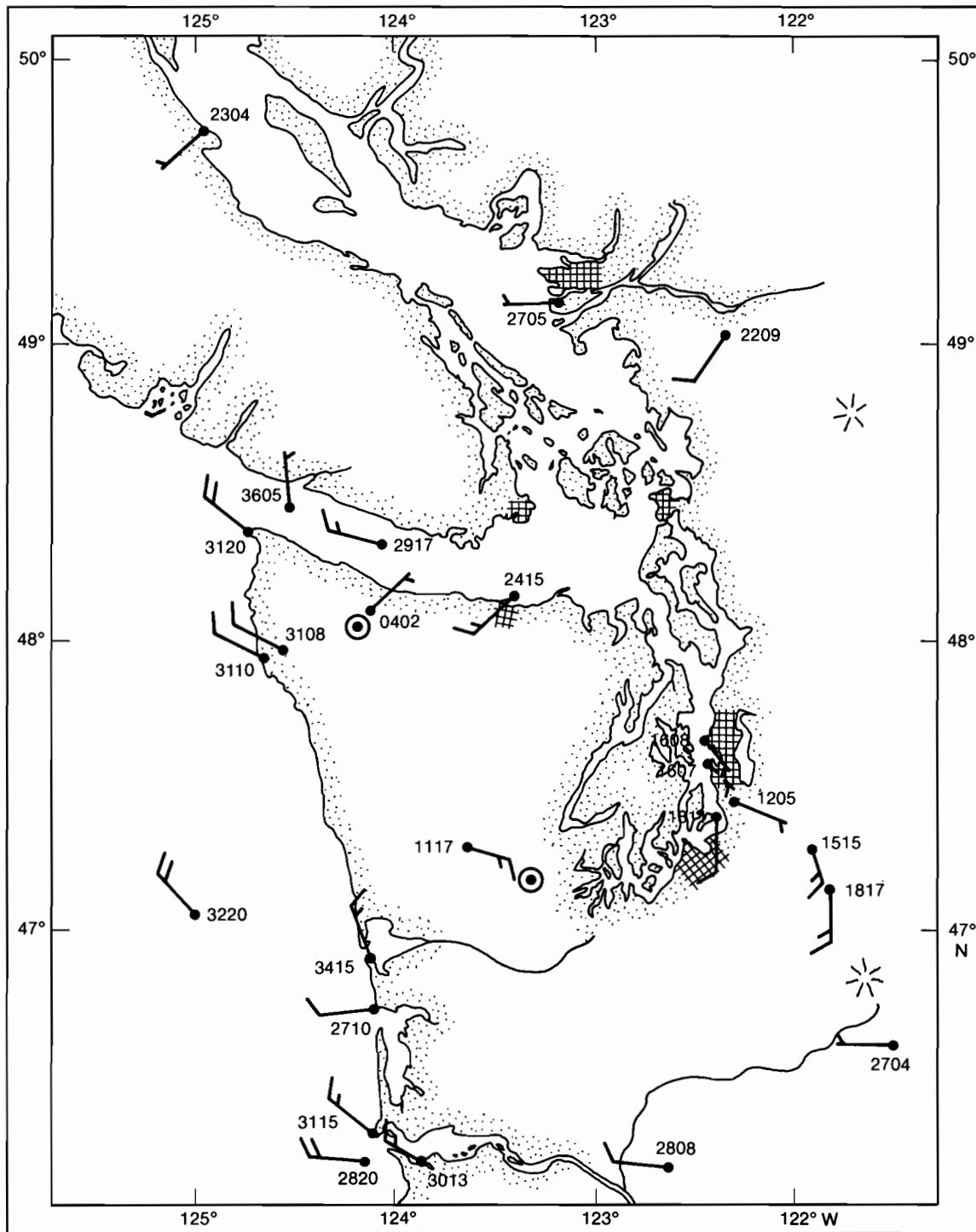


Figure 31.—Local wind observations, 9 December 1976, 1200 GMT.

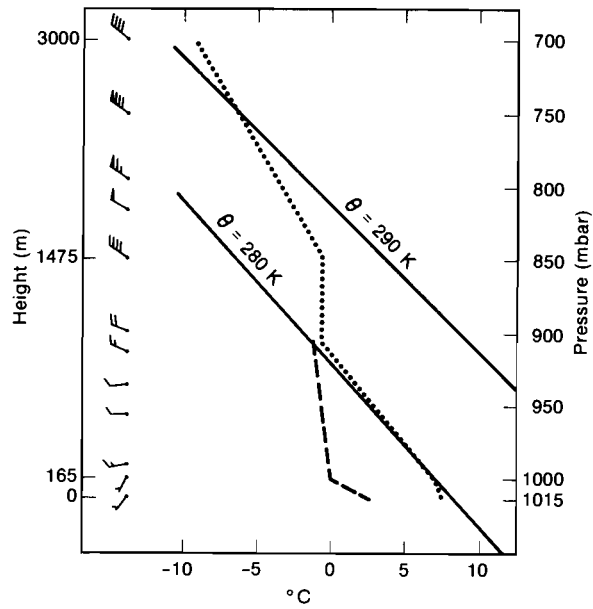


Figure 32.—Temperature sounding (· · · ·), dew point (---), and potential temperature (—) at Quillayute (Washington coast) for 1200 GMT and wind at McChord Air Force Base (Puget Sound) for 1400 GMT, 9 December 1976.

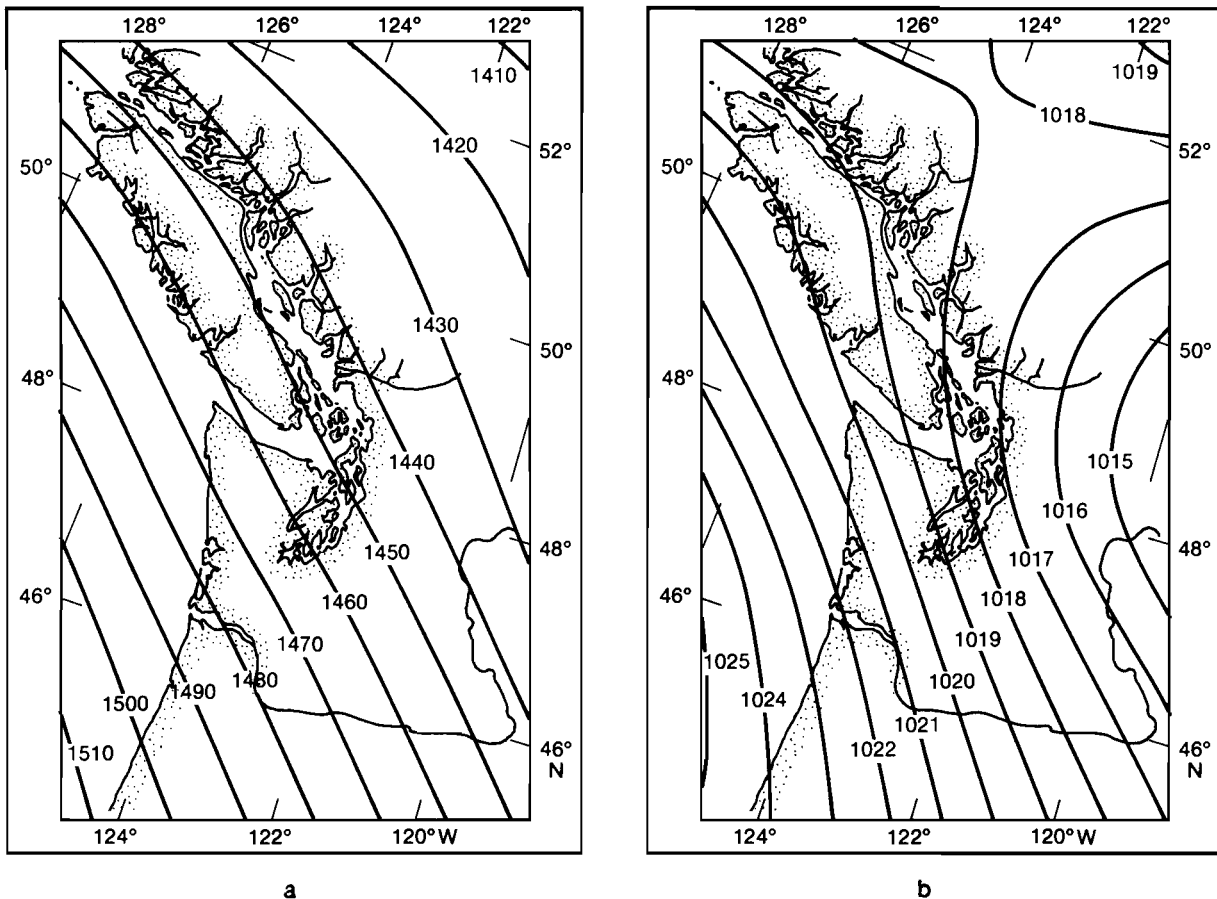
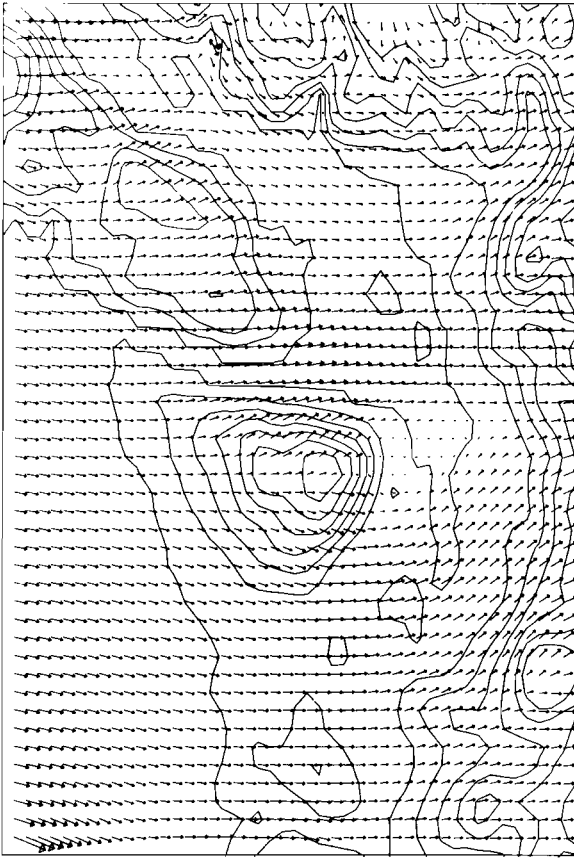


Figure 33.—Objective analysis of (a) 850-mbar heights and (b) sea level pressure on 9 December 1976, 1200 GMT.



10 m s<sup>-1</sup>

Figure 34.—Velocity vector plot of model winds for northwest flow.

## 7. REFERENCES

- Brown, R. A. (1974): A simple momentum integral model. *J. Geophys. Res.* 79:4076-4079.
- Holbrook, J. R., and D. Halpern (1978): Variability of near-surface currents and winds in the western Strait of Juan de Fuca. Pacific Marine Environmental Laboratory, Seattle, Washington. Unpublished manuscript.
- Keyser, D., and Anthes, R. (1977): The applicability of a mixed-layer model of the planetary boundary layer to real-data forecasting. *Mon. Wea. Rev.* 105:1351-1371.
- Lavoie, R. (1972): A mesoscale numerical model of lake-effect storms. *J. Atmos. Sci.* 29:1025-1040.
- Lavoie, R. (1974): A numerical model of tradewind weather on Oahu. *Mon. Wea. Rev.* 102:630-637.
- Ogura, Y., and N. W. Phillips (1962): Scale analysis of deep and shallow convection in the atmosphere. *J. Atmos. Sci.* 19:173-179.
- Reed, J. (1931): Gap winds of the Strait of Juan de Fuca. *Mon. Wea. Rev.* 59:373-376.
- Shuman, F. G. (1957): Numerical methods in weather prediction, II: smoothing and filtering. *Mon. Wea. Rev.* 85:357-361.
- Stull, R. B. (1976): Mixed-layer depth model based upon turbulent energetics. *J. Atmos. Sci.* 33:1268-1278.

## 6. ACKNOWLEDGMENTS

This study was supported jointly by the Marine Ecosystems Analysis (MESA) Puget Sound Project and the Outer Continental Shelf Environmental Assessment Program (OCSEAP) to assist in providing wind field information for oil spill trajectory calculations, and by the Marine Services Program at the Pacific Marine Environmental Laboratory (PMEL), which aids National Weather Service marine prediction along the west coast and the Gulf of Alaska.

We wish to thank Robert Anderson and his colleagues at the Seattle National Weather Service Forecast Office for their collaboration in the field program and in compiling the routine observation data sets, and Jim Holbrook of PMEL for making available his anemometer observations and discussing their implications.

## APPENDIX: Derivation of Boundary Layer Equations

We shall write the equations of motion for deviation from a steady reference state. If the reference state changes only very little with height, it is possible to use the Boussinesq approximation, but with potential temperature as the thermal variable (Ogura and Phillips, 1962).

The momentum equation is

$$\begin{aligned} \frac{\partial \bar{v}}{\partial t} + \bar{v} \cdot \nabla \bar{v} &= w \frac{\partial \bar{v}}{\partial z} + f \bar{k} x \bar{v} + c_p \theta_0 \nabla \pi \\ &= -\frac{\partial}{\partial z} (\overline{v'w'}) \end{aligned} \quad (\text{A1})$$

where  $\pi \equiv \left(\frac{P}{P_0}\right)^\chi$ ,  $\chi = R/c_p$ .

The hydrostatic equation is

$$c_p \theta \frac{\partial \pi}{\partial z} = -g. \quad (\text{A2})$$

The equation of continuity is

$$\nabla \cdot \bar{v} + \frac{\partial w}{\partial z} = 0. \quad (\text{A3})$$

The first law of thermodynamics is approximated by

$$\frac{\partial \theta}{\partial t} + \bar{v} \cdot \nabla \theta + w \frac{\partial \theta}{\partial z} = -\frac{\partial}{\partial z} (\overline{w'\theta'}). \quad (\text{A4})$$

In these equations  $\bar{v}$  is Reynolds' averaged horizontal velocity vector,  $\bar{v}'$  is the deviation velocity,  $\theta$  is potential temperature, and  $\theta_0$  is the potential temperature of the reference state (constant). The other terms are defined in the usual meteorological sense.

We simplify the hydrostatic equation (A2) in the following way:

$$c_p \frac{\partial \pi}{\partial z} = -\frac{g}{\theta} \equiv -g \frac{1}{\theta_0} \left(1 - \frac{\theta''}{\theta_0}\right),$$

where  $\theta'' = \theta - \theta_0$ .

If we define  $\pi_0$  such that

$$c_p \frac{\partial \pi_0}{\partial z} = -\frac{g}{\theta_0},$$

then

$$c_p \frac{\partial \pi''}{\partial z} = \frac{g}{\theta_0} \frac{\theta''}{\theta_0}$$

where  $\pi'' = \pi - \pi_0$ .

Since  $\pi_0$  is a function of  $z$  only, we can rewrite eq. (A1)

$$\begin{aligned} \frac{\partial \bar{v}}{\partial t} + \bar{v} \cdot \nabla \bar{v} + w \frac{\partial \bar{v}}{\partial z} \\ + f \bar{k} x \bar{v} + c_p \theta_0 \nabla \pi'' \\ = -\frac{\partial}{\partial z} (\overline{v'w'}). \end{aligned} \quad (\text{A6})$$

We shall use eqs. (A3), (A4), (A5), and (A6) for describing the flow field in the well-mixed layer.

We now integrate (A4) and (A6) through the mixed layer. The basic equations then become

$$\begin{aligned} \frac{\partial \bar{v}}{\partial t} + \bar{v} \cdot \nabla \bar{v} + f \bar{k} x \bar{v} + \frac{c_p \theta_0}{h-D} \int_D^h \nabla \pi'' dz \\ = -(\overline{v'w'_h} - \overline{v'w'_s})/(h-D), \end{aligned} \quad (\text{A7})$$

$$\frac{\partial \theta}{\partial t} + \bar{v} \cdot \nabla \theta = -(\overline{w'\theta'_h} - \overline{w'\theta'_s})/(h-D). \quad (\text{A8})$$

In addition, the mass continuity equation, by definition, can be written

$$\frac{\partial h}{\partial t} + \nabla \cdot (h-D)\bar{v} = E \quad (\text{A9})$$

where  $E$  is the net entrainment rate at which the well-mixed layer gains mass from the free atmosphere.

Using the hydrostatic equation, we evaluate the vertically integrated pressure gradient force:

$$\begin{aligned} -\frac{c_p \theta_0}{(h-D)} \int_D^h \nabla \pi'' dz &= -c_p \theta_0 \nabla \pi_H'' \\ + \frac{g}{\theta_0} (H-h) \nabla \theta_H'' - \frac{g}{\theta_0} (\theta_h'' - \theta_s'') \nabla h \\ + \frac{g}{\theta_0} \frac{1}{2} (h-D) \nabla \theta'' \end{aligned} \quad (\text{A10})$$

where subscript  $H$  denotes the top of the model atmosphere.

For the convenience of finite differencing, eq. (A8) is written in a flux form:

$$\begin{aligned} \frac{\partial}{\partial t} (h-D)\theta + \nabla \cdot (h-D)\bar{v}\theta - \theta E \\ = -(\overline{w'\theta'})_h + (\overline{w'\theta'})_s. \end{aligned} \quad (\text{A11})$$

In deriving the equation, eq. (A9) was used. The momentum equation (A7) was also put in flux form.

Integrating eq. (A1) and (A4) across the jump between the PBL and inversion layer using Leibnitz' rule, we obtain relations

$$(\bar{v}'w')_h = -E\Delta\bar{v} \quad (\text{A12})$$

$$\text{and } (w'\theta')_h = -E\Delta\theta \quad (\text{A13})$$

where  $\Delta\bar{v} = \bar{v}_+ - \bar{v}_-$  and  $\Delta\theta = \theta_+ - \theta_-$ .

The flux form of (A9) with the substitution of (A10), equations (A9) and (A11), and entrainment relations (A12) and (A13) form a closed set of equations, (1), (2), and (3) in the text, given that the entrainment rate can be parameterized in terms of the mixed layer variables.